242
6-23-75

Dr-1399

UCRL-51818

DEVELOPMENT AND EVALUATION OF RADON SEALANTS FOR URANIUM MINES

H. G. Hammon
K. Ernst
J. R. Gaskill
J. C. Newton
C. J. Morris

May 21, 1975

Prepared for U.S. Energy Research & Development Administration under contract No. W-7405-Eng-48

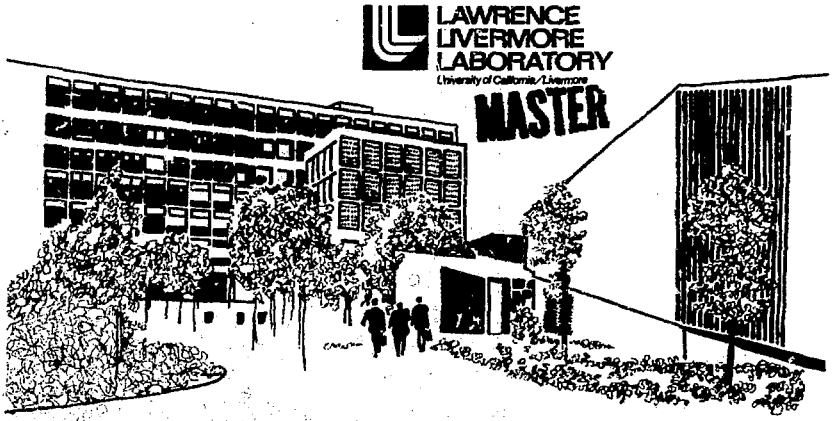

DISTRIBUTION OF THIS DOCUMENT UNLIMITED

NOTICE

"This report was prepared as an account of work sponsored by the United States Government. Neither the United States nor the United States Energy Research & Development Administration, nor any of their employees, nor any of their contractors, subcontractors, or their employees, makes any warranty, express or implied, or assumes any legal liability or responsibility for the accuracy, completeness or usefulness of any information, apparatus, product or process disclosed, or represents that its use would not infringe privately-owned rights."

Printed in the United States of America
Available from
National Technical Information Service
U. S. Department of Commerce
5285 Port Royal Road
Springfield, Virginia 22151
Price: Printed Copy $___*; Microfiche $2.25

*Pages	NTIS Selling Price
1-50	$4.00
51-150	$5.45
151-325	$7.60
326-500	$10.60
501-1000	$13.80

USBM Contract Number HO232047

TID-4500, UC-41
Health and Safety

LAWRENCE LIVERMORE LABORATORY
University of California/Livermore, California/94550

UCRL-51818

DEVELOPMENT AND EVALUATION OF RADON SEALANTS FOR URANIUM MINES

H. George Hammon
Klaus Ernst
James R. Gaskill
John C. Newton
C. J. Morris

USBM CONTRACT REPORT HO232047
May 29, 1975

DEPARTMENT OF THE INTERIOR
BUREAU OF MINES
WASHINGTON, D.C.

NOTICE

The views and conclusions contained in this document are those of the authors and should not be interpreted as necessarily representing the official policies or recommendations of the Interior Department's Bureau of Mines or of the U.S. Government.

NOTICE

This report was prepared as an account of work sponsored by the United States Government. Neither the United States nor the United States Energy Research and Development Administration, nor any of their employees, nor any of their contractors, subcontractors, or their employees, makes any warranty, express or implied, or assumes any legal liability or responsibility for the accuracy, completeness or usefulness of any information, apparatus, product or process disclosed, or represents that its use would not infringe privately owned rights.

Foreword

This report was prepared by Lawrence Livermore Laboratory, Livermore, California under USBM Contract Number H0232047. The contract was initiated under the Metal and Nonmetal Health and Safety Research Program. It was administered under the technical direction of SMRC with Mr. John C. Franklin acting as the Technical Project Officer. Mr. Frank Pavlich was the contract administrator for the Bureau of Mines.

This report is a summary of the work recently completed as part of this contract during the period October, 1972, to February, 1975. This report was submitted by the authors on May 29, 1975.

Work was performed under the auspices of the U.S. Energy Research & Development Administration. Reference to a company or product name does not imply approval or recommendation of the product by the University of California or the U.S. Energy Research & Development Administration to the exclusion of others that may be suitable.

The authors acknowledge gratefully the assistance of many others in this work, especially Floyd Momyer for direct radon permeation measurements, James S. Johnson for toxicity evaluations, and Norriss Hetherington for statistical and mathematical analysis.

Contents

Foreword ii
Introduction 1
Summary and Conclusions 1
Experimental Work 3
Task 1: Coating Selection and Preparation 3
Task 2: Measurement of Permeability and Diffusion Constants 3
1. Dynamic Method Using a Mass Spectrometer as a Gas Detector 3
2. Use of Dow Cell for Permeability Measurements 5
3. Direct Determination of Radon Permeability 5
Results and Discussion of Permeability Study 6
Modification of Coatings 10
Effects of Pigments in Coatings 10
Effects of Crosslinking 10
Thickening Agents 11
Correlation of Permeability with Polymer Structure 11
Permeability of Uranium Ore 14
Task 3: Evaluation of Toxicity of Coatings 14
Smoke Chamber Studies of Coatings 15
Preparation of Specimens 15
Smoke Chamber Tests 15
Flash Points of Coatings 16
Laboratory Pyrolysis Test Under Non-Flaming Conditions 18
Results and Discussion 18
GC/MS Analysis of Volatiles from Polymers 21
Toxicological Evaluation of Coatings 23
References 24
Appendix A: Tables and Figures 25
Appendix B: Computer Program (PDP-8) for Calculation of Permeability Coefficients from Dow Cell Data. 54
Appendix C: Direct Determination of Radon Permeability through Polycarbonate Film 57

Introduction

Uranium miners have been shown to develop lung cancer in direct proportion to the time of exposure in the mine and the concentration of radioactivity (cumulative working level).[1] Radon gas is continually evolved from the uranium ore, but because of its short half-life, 3.82 days, it is soon decomposed into particulate daughter products, which, along with the dust in the mine, become deposited in the miners' lungs. At present, massive ventilation is the only effective method of reducing the radioactivity concentration in the mines. However, the Bureau of Mines is evaluating the possibility of using coatings on the mine walls that will have sufficiently low permeability to radon that the gas will decompose into the particulate daughter products before it can permeate the coating. Permanently trapped in the coating, the daughter products would be prevented from dispersing in the mine atmosphere.

Lawrence Livermore Laboratory was asked to aid in this investigation. The direct determination of radon permeability is more difficult than that of the other noble gases because of the short half-life of the gas and radioactive contamination of the apparatus. We felt that it should be possible to estimate radon permeation coefficients from other noble gas permeation coefficients. It was noted that the log of the diffusion constants for helium, neon, argon, and krypton, as reported by Meares[2,3] plotted to a straight line against the square of the gas molecular diameter. The log of the permeation coefficients also plotted to a straight line against the square of the gas molecular diameter. Thus, by determining the permeation coefficients of such gases as argon and krypton through various films and coatings, it appeared likely that radon permeation coefficients could be estimated. In addition, we felt it should be possible to find some relationship between polymer structure and the noble gas permeation coefficient that would aid in the selection of coatings materials as radon barriers.

As the program progressed, we were asked to evaluate selected coatings for their possible toxicity during application or a mine fire. As the coatings were of industrial origin, it was possible that they might contain volatile materials that would pose a toxicological hazard to personnel while applying coatings to the mine walls. Also, a mine fire might be made more hazardous by dense smoke from the coating or toxic materials emitted during its pyrolysis.

Summary and Conclusions

The purpose of this study was to evaluate selected coatings as radon barriers in uranium mines; first on their effectiveness in reducing radon permeation, and second on the basis of their potential toxicity during application or in a possible mine fire. Hopefully, this information would be helpful in developing coatings more effective than those commercially available.

The program was organized in three tasks: (1) Film Selection and Preparation; (2) Measurement of Permeability; and (3) Evaluation of Toxicity of Coatings.

Films for the permeation study were selected from commercially available polymer systems of known chemical composition. Coating systems were selected on the basis of their chemical composition using our own permeability data or published data to aid in selections; other coatings previously evaluated at Bureau of Mines were also studied. In agreement with the Bureau of Mines seven coatings were selected for full evaluation, including smoke chamber and toxicity studies. Two more were added later for smoke chamber study only. Permeation coefficients of the films and coatings to noble gases were determined. When the log of the permeation coefficients for argon, krypton and xenon is plotted against the square of the molecular diameter a linear relationship is obtained. Thus, a straight-line extrapolation of this line permits the estimation of the permeability coefficient for radon. The latter may be undesirable as surface coatings because they yield large amounts of hydrogen

chloride ($HC\ell$) when exposed to heat or fire; however, they produce negligible amounts of smoke. They might be useful as penetrating compositions to bond loose uranium ore. The one-component polyester develops only light smoke, but would be hazardous during application because it releases relatively large amounts of styrene vapors, and has a low flash point.

The furan coating has very low permeability to noble gases, and develops negligible amounts of smoke. However, it has an objectionable odor which would be difficult to mask, and its black color might be undesirable.

Three epoxy coatings were evaluated. Two of these were unpigmented; they developed dense smoke when exposed to heat or fire. The pigmented epoxy coating produced only a light smoke, and its vapors contained no toxic components.

Toxic components evolved from the uncured polymer systems were determined by gas chromotography/mass spectrography (GC/MS). The only materials of toxicological significance that were found were vinylidene chloride (a suspected carcinogen) in the vinylidene chloride copolymer, vinyl chloride (a carcinogen) in one of the unpigmented epoxy coatings, and epichlorohydrin (a sensitizer), in the same epoxy coating.

Pyrolysis studies were made on the cured coatings. Other than carbon monoxide and $HC\ell$ no significant quantities of other toxic species were found. Carbon monoxide was not generated from any of the coatings in amounts that would be large compared with those that would be evolved from other materials usually involved in a mine fire, such as wood, diesel fuel, and waste materials.

In ranking the coatings studied, we should note that they represent only a few of such commercial coatings available; other manufacturers may make similar coatings. Also, the ranking gives relatively little weight to permeability, as all are adequate to stop radon in the normal thickness of application, providing a continuous coating is effected. Finally, coatings 8 and 9 were evaluated only in the smoke chamber, but produced more smoke than most of the other coatings under these conditions. Thus, we rank the coatings in decreasing order of overall effectiveness as follows:

Name and Type	Comments
1. HydrEpoxy 300, pigmented water-dispersed epoxy	
2. Resitron II, furan (catalyzed furfuryl alcohol polymer)	Bad odor
3. Essex Polyester, pigmented one-component styrenated polyester	Flammable; contains styrene
4. Aerospray 70, plasticized polyvinyl acetate latex	Possible smoke problem
5. Saran XD-7151, vinylidene chloride copolymer	Liberates hydrogen chloride in possible fire
6. EpiRez WD-510/EpiCure 872, unpigmented water-dispersed epoxy	Possible smoke problem
7. WSU-118, modified epoxy	Possible smoke problem
8. Promulsion 200, unidentified composition	Possible smoke problem
9. Hydro Seal, acrylic emulsion	Possible smoke problem

We have calculated that virtually all coatings with permeation constants lower than 10^{-10} $cm^3_{STP} \cdot cm/s \cdot cm^2 \cdot cm$ Hg and thicknesses between 5 and 10 mil will provide nearly 100% effectiveness. The selection of a suitable coating then ought to be based on other factors such as cost/m^2, vapor toxicity during application, ability to bind to the uranium ore in continuous films free of pin-holes etc. Obviously, any openings in the mine shafts and tunnels which are not covered with a film or any discontinuities of the film will act like the spillway on a water dam, i.e., the radon contained behind the barrier will flow out into the tunnel.

Experimental Work

The study of radon sealants for uranium mines was organized as three tasks: (1) Coating Selection and Preparation; (2) Measurement of Permeability and Diffusion Constants; and (3) Evaluation of Toxicity of Coatings. Although there was overlapping of these tasks, this was also the chronological order in which the study was made.

TASK 1: COATING SELECTION AND PREPARATION

Many of the coatings evaluated at LLL had previously been studied at Bureau of Mines, SMRC. Additionally, we surveyed the chemical industry and obtained specimens of coatings materials for evaluation. As much as possible, the composition of the coatings was obtained from the manufacturer. Permeability studies were also made on commercial films of known composition, and these results were used as a basis for selection of coatings.

Most of the coatings were prepared by drawdown from solution or latex using a doctor blade on a substrate of known permeability. This substrate was usually a polyethylene ionomer (Surlyn A). This material had high permeability and wetted better than conventional polyethylene. The coatings were allowed to dry thoroughly at room temperature and were conditioned for several days at about 50% relative humidity. The thickness of unsupported coatings or coatings on the Surlyn A substrate was measured with an electronic micrometer and averaged values were rounded off to the nearest 0.025 mm (0.0001 in.).

Coatings for evaluation in the LLL/NBS Smoke Chamber were applied, usually by spraying, to the surface of 73 X 73 X 25 mm cement-asbestos board specimens. In some cases, similar size specimens were cut from low-grade uranium ore and were coated for smoke-chamber study. Results with coatings on uranium ore specimens were essentially the same as with cement-asbestos board specimens. It was costly to cut the ore specimens and their uranium content required special monitoring procedures. Therefore, most determinations were made on cement-asbestos board specimens. Coatings on the cement-asbestos board or uranium ore specimens were measured indirectly by bonding a thin steel steeh to the surface of a similar specimen, coating it at the same time and in the same manner as the speciments to be evaluated in the smoke chamber, and measuring the thickness of the cured coating with a magnetic coating thickness gage.

TASK 2: MEASUREMENT OF PERMEABILITY AND DIFFUSION CONSTANTS

1. Dynamic Method Using a Mass Spectrometer as a Gas Detector

In this dynamic technique a small mass spectrometer (a converted CEC21-614 Residual Gas Analyzer) serves as gas detector. The specificity, sensitivity and precision are superior to most other detectors. For thin film (up to 15 mils) this method gives results rapidly, and interfering membrane outgassing and desorption gases can be distinguished from the permeant. The presence of pinholes in, or leaks around, the membrane is readily recognized. A schematic of the measurement system is shown in Fig. 1. The specially designed permeation cell is connected to the ion source via an isolation valve. In the open position the flow impedance of the valve port is negligible relative to the flow impedance of the membrane. By using two Viton O-rings and continuously pumping on the volume between the O-rings, air leaks are virtually eliminated.

The O-rings are vacuum baked before assembling the cell to remove dissolved gases and water vapor. This cell can be heated to about 150°C and the membrane thickness can be varied from 1 mil to about 65 mils. In operation, the permeation cell is evacuated on both sides of the membrane and a spectrum of the residual gases is obtained. If any of these gases are identical to the permeant to be used (the test gas) evacuation continues until the background is negligible. If this requires too much time, the outgassing and/or desorption rates are measured as function of time to be used as correction factors to the permeation rate. The isolation valve to the spectrometer is

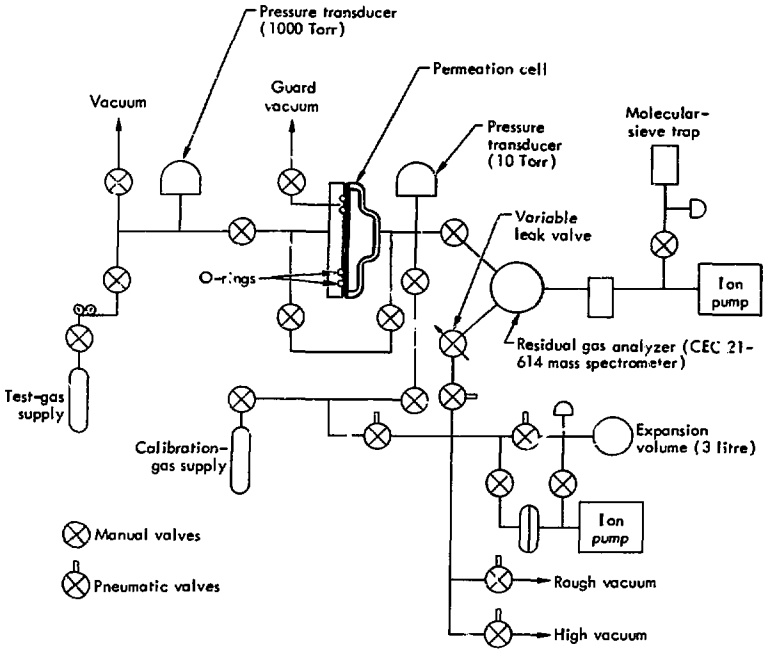

Fig. 1. Diagram of the mass spectrometer and associated apparatus that was used for measurement of permeability constants.

then opened and the test gas is applied at a known pressure (P_1) on the in-going side of the membrane. A suitable ion peak (m/e = 4 for helium; m/e = 40 for Ar; m/e = 83, 84 or 86 for Kr) is continuously monitored until the recorder trace or digital output reaches a steady state value.

The system is calibrated by measuring the mass spectrometer's electrometer response to a known, constant flow of the test gas which furnishes the sensitivity (S). The steady-state permeation rate ($\dot{Q}$) is obtained from the relation

$$\dot{Q} = S \cdot V_{ss} \ ,$$

where

$\dot{Q}$ = permeation rate (cm^3_{STP}/s)

S = sensitivity ($cm^3_{STP}/s \cdot mV$)

V_{ss} = electrometer signal at steady state (mV).

From this, the permeation coefficient is calculated using the following equation:

$$P = \dot{Q} \cdot d/A\Delta p \ ,$$

where

d = membrane thickness (cm)

A = membrane area (cm^2)

$\Delta p = p_1 - p_2 \simeq p_1$ = test gas pressure (cm Hg)

P = permeation coefficient ($cm^3_{STP} \cdot cm/s \cdot cm^2 \cdot cm\ Hg$)).

From a single experiment we can also calculate the diffusion constant (D) by the method of Pasternak[4] if the complete permeation curve from zero transmission to the steady state value is obtained. Since

$$P(T) = D(T)\, s(T),$$

the solubility (s) can be calculated with P and D determined. All three terms are temperature dependent. Experiments at different temperatures permit the measurement of the temperature coefficients.

2. Use of Dow Cell for Permeability Measurements

Determinations of permeability coefficients using the mass spectrometer often required long times, expecially with low permeability films and coatings and with the higher molecular weight gases such as kyrpton and xenon. Therefore, we made many of our determinations with a Dow film permeability cell, as described in ASTM D-1434-66. A computer program was written for a PDP-8 to calculate permeation coefficients from the experimental data; the program is shown in Appendix B.

3. Direct Determinations of Radon Permeability

Radon permeation measurements are more difficult to make than those of other noble gases for a number of reasons. For most polar materials, the radon permeation rate will be slow due to the larger gas molecule and its slower diffusion rate. It has a relatively short half life, thus deposits its daughter products in the measuring apparatus. We did not want to so contaminate the mass spectrometer or the Dow cell. Therefore, direct determination of radon permeation through polyethylene and through polycarbonate films was made using radiochemical techniques with apparatus made for the purpose from 80-mm pyrex glass tubing. Radon, derived from a radium solution, was admitted to one side of the apparatus, and allowed to permeate the film which separated the apparatus into two chambers. The gas which permeated the film was determined on the other side by alpha counting. Complete details of the determination of the radon permeability coefficient of polycarbonate film are described in Appendix C by Dr. Floyd Momyer, who was in charge of this phase of the work.

RESULTS AND DISCUSSION OF PERMEABILITY STUDY

The permeation coefficients of some commercial films are listed in Table 1 and the permeation coefficients of some supported coatings are listed in Table 2. A complete listing of the permeation coefficients of the supported coatings will be found in Table A-1 in Appendix A. Some of these data are plotted in Figs. 2 and 3 as the logs of the permeation coefficients vs the square of the diameter of the permeant gas. In general, good straight line fits were obtained for argon, krypton, and xenon permeation coefficients, although the helium and neon permeation coefficients did not usually fit well with the other data. Direct measurements of the radon permeation coefficients were made only through polyethylene and polycarbonate films. As may be seen from Fig. 2, these values agreed well with values that would be predicted by extrapolation of the argon, krypton, and xenon values.

The permeation coefficients for noble gases through polyethylene and Surlyn A increase with increasing gas molecular weight and diameter. Similar effects have been reported for neon and argon permeation through ethylene-propylene copolymers, styrene-butadiene copolymers, and a cis-polybutadiene[5], for neon, argon, krypton, and xenon through natural rubber[6], and for neon, argon, krypton, and xenon through silicone rubber[7]. In polymers of higher cohesive energy

Table 1. Permeation coefficients of commercial films.

Film	Gas	Permeation coefficients	
		$\frac{cm^3_{STP} \cdot cm}{sec \cdot cm^2 \cdot cm\ Hg}$	$\frac{nm^2}{Pa \cdot s}$
Polyethylene	He	6.7×10^{-10}	50
	Ar	3.4×10^{-10}	25
	Kr	4.5×10^{-10}	34
	Xe	8×10^{-10}	60
	Rn	1.5×10^{-9}	113
Surlyn A	Ne	2.0×10^{-10}	15
(polyethylene ionomer)	Ar	1.3×10^{-10}	9.8
	Kr	1.5×10^{-10}	11
	Xe	1.9×10^{-10}	14
Polycarbonate	He	1.5×10^{-9}	113
	Ar	5.5×10^{-11}	4.1
	Kr	5×10^{-11}	3.8
	Xe	2×10^{-11}	1.5
	Rn	1.8×10^{-11}	1.4
Polyvinylchloride,	He	4.0×10^{-10}	30
unplasticized	Ar	7.0×10^{-12}	0.53
	Kr	3.5×10^{-12}	0.26
	Xe	4×10^{-13}	0.03
Phenoxy	Ne	2.5×10^{-11}	1.9
	Ar	2.6×10^{-12}	0.20
	Kr	1.1×10^{-12}	0.08
	Xe	2.1×10^{-13}	0.016

Table 2. Permeation coefficients of supported coatings.

Description	Permeation coefficients, $\frac{cm^3_{STP} \cdot cm}{s \cdot cm^2 \cdot cm\ Hg}$, $\frac{nm^2}{Pa \cdot s}$		
	Ar	Kr	Xe
Polymethyl acrylate, low viscosity	3.9×10^{-11} (2.9)	N.D.	N.D.
Vinyl chloride copolymer, latex	6.0×10^{-12} (0.45)	N.D.	N.D.
Vinylidene chloride copolymer, latex	4.4×10^{-13} (0.033)	2.2×10^{-13} (0.017)	8.9×10^{-14} (0.0067)
Epoxy, pigmented, from water dispersion	7.3×10^{-12} (0.55)	6.8×10^{-12} (0.51)	5.0×10^{-12} (0.38)
Epoxy, not pigmented, from water dispersion	1.1×10^{-11} (0.83)	7.7×10^{-12} (0.58)	3.5×10^{-12} (0.26)
Polyvinylacetate, plasticized, latex	2.4×10^{-11} (1.8)	1.1×10^{-11} (0.83)	1.9×10^{-12} (0.14)
Styrenated polyester, pigmented	1.7×10^{-10} (13)	N.D.	N.D.

density*, however, the permeation coefficients of the noble gases decrease with increasing gas molecular weight and diameter, as shown by our data and the data of Meares[2,3].

It has been shown[8] *that* $P = DS$, *where* P *is the* permeation coefficient, D is the diffusion coefficient, and S is the solubility coefficient, provided D is constant. Up to pressures of 1 or 2 atmospheres, the solubility of the noble gases in polymers obeys Henry's law, i.e. $C = Sp$, where

C = concentration of gas dissolved in unit volume of polymer (cm^3_{STP}/cm^3)

p = partial pressure of noble gas in contact with the polymer (1 atm)

s = solubility coefficient $\left(\frac{cm^3_{STP}}{cm^3 \cdot atm}\right)$.

For gases that dissolve only sparingly, the solubility coefficient (S) is a constant. Once dissolved the permeated molecules diffuse to the other side of the membrane. The driving force is the concentration difference that exists between the incoming and outgoing membrane surfaces. The flux of permeant (J) per unit membrane surface area is then given by

$$T = D\ (C_{in} - C_{out})/d$$

or

$$J = SD\ (p_{in} - p_{out}/d,$$

where

d = thickness of the membrane (cm)

D = diffusion coefficient $\left(\frac{cm^2}{s}\right)$

J = flux of permeant $\left(\frac{cm^3_{STP}}{s \cdot cm^2}\right)$

The diffusion coefficient (D) is essentially a constant for sparingly soluble gases because the membrane structure is not perturbed by the dissolved molecules. Up to and near atmospheric pressures, the diffusion of noble gases in polymers is independent of concentration. This is mainly because of the very low concentrations encountered at all normal pressures, but it also reflects the comparative lack of interaction between these gases and the polymer.

At pressures of 1 or 2 atmospheres, the solubility of the gases in the polymers obeys Henry's law. In

*The cohesive energy density (CED) is approximately equal to the heat of vaporization or sublimation at constant volume and can be estimated from thermodynamic data.

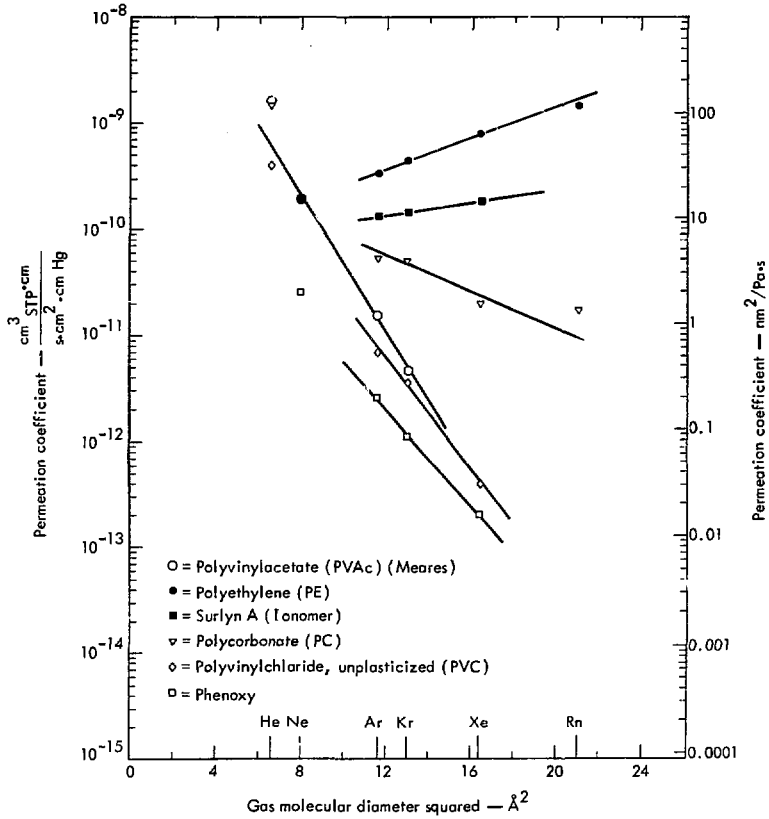

Fig. 2. Permeation coefficients of films vs the square of the gas molecular diameter.

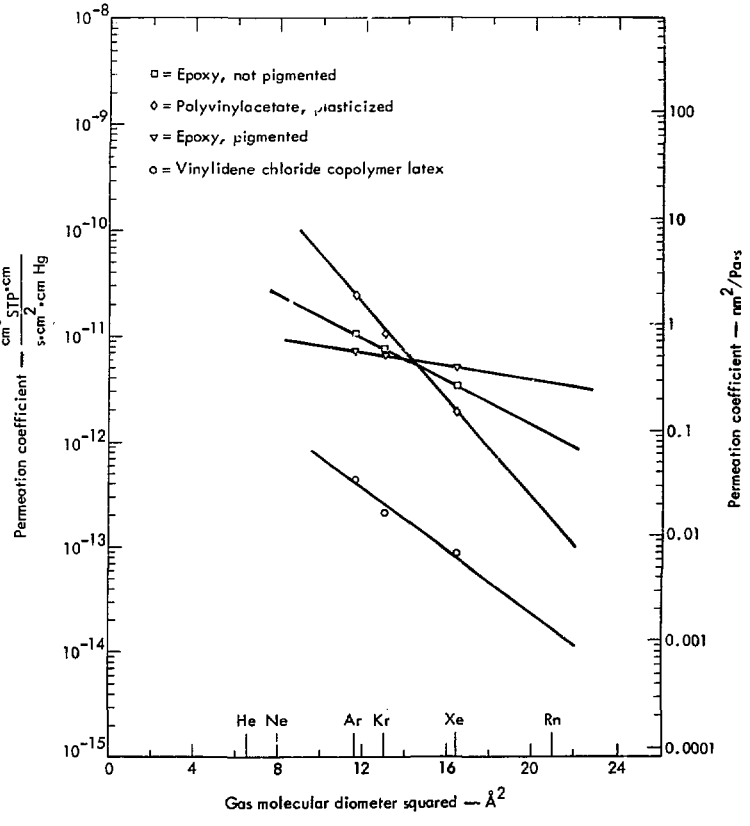

Fig. 3. Permeation coefficients of coatings vs the square of the gas molecular diameter.

the generally accepted picture of the activated diffusion process, larger holes need to be formed in the polymer for the diffusion of larger molecules. These larger holes require a larger energy for their formation, thus the activation energy will be larger for the diffusion of larger molecules and the diffusivity will be smaller. This has been found to be true. However, the solubility increases with increasing gas molecular weight and has been shown[9,10] to be directly related to the critical temperatures of the gas. Solubility of simple gases in hydrocarbon polymers has been found to be directly proportional to the volume fraction of amorphous polymer;[11] however, introduction of polar groups decreases solubility. Thus, in looking at the permeability coefficients of the noble gases in a particular polymer film, if the solubility coefficient increases more (in going from one noble gas to the next in order of increasing molecular weight) than the diffusion coefficient decreases, the net effect on the permeation coefficient is an increase.

Modification of Coatings

Effects of Pigments in Coatings

Many of the coatings evaluated in this study were pigmented as obtained from the manufacturer. In some cases, it was possible to compare pigmented with non-pigmented coatings, but, as in the case of the epoxy coatings reported (compare the HydrEpoxy coatings with the EpiRez/EpiCure coatings) there appeared to be little difference between them. It would be reasonable to expect, however, that some pigments would reduce the permeability of the coating by an overlapping or leafing structure in the dried coating. Two pigments were selected with this effect in mind: a leafing aluminum pigment, and powdered mica. In a Saran latex (Dow XD-4624), the addition of the leafing aluminum pigment reduced the permeation coefficient by about a factor of 2, but the mica modified coating had a permeation coefficient higher than the unmodified coating by about a factor of 10. The pigments were also studied in an ethylene/vinyl chloride copolymer, Monflex 4514. The permeation coefficient to argon of the mica modified Monflex 4514 was found to be 1.2×10^{-11}, about half the value found for the latex compound with aluminum pigment, but still twice as high as the unpigmented latex. Because the permeability coefficients appeared to be affected more by the choice of the base polymer than by pigment compounding, this work was not carried further. Data are listed in Table 3.

Effects of Crosslinking

Crosslinking of polymer film has been shown to reduce permeation, apparently by reduction in the diffusion constant.[12-15] No direct attempt was made in this program to reduce permeation by crosslinking

Table 3. Effects of pigments in coatings.

Coating (type)	Pigment	Permeation coefficient of coating	
		$\frac{cm^3_{STP} \cdot cm}{s \cdot cm^2 \cdot cm\ Hg}$	$\frac{nm^2}{Pa \cdot s}$
Saran XD-4624 (Vinylidene chloride copolymer)	None	4.4×10^{-13}	0.033
Saran XD-4624 (Vinylidene chloride copolymer)	Leafing Aluminum	1.9×10^{-13}	0.014
Saran XD-4624 (Vinylidene chloride copolymer)	Ground mica	4.2×10^{-12}	0.32
Monflex 4514 (ethylene/vinyl chloride copolymer)	None	6.0×10^{-12}	0.45
Monflex 4514 (ethylene/vinyl chloride copolymer)	Leafing aluminum	2.5×10^{-11}	1.9
Monflex 4514 (ethylene/vinyl chloride copolymer)	Ground mica	1.2×10^{-11}	0.9

because of the difficulty of introducing crosslinking agents that would be effective in room temperature cures. However, we did observe a definite lowering, by about an order of magnitude, in the permeation coefficient of a HydrEpoxy coating that was retested after standing for several months. We attribute this to the increase in crosslinking taking place in the room temperature curing epoxy. A polyvinyl acetate coating prepared at the same time as the epoxy coating showed no change on remeasurement after standing.

Thickening Agents

Some of the coatings were low in viscosity and tended to sink into porous substrates such as the uranium ore. If this happened, a coherent film was not formed and the coating was not a good barrier. Thickening agents such as polyvinyl alcohol solution or carboxymethyl cellulose were recommended by the manufacturer. Used at the recommended levels, these thickening agents did not change the permeation coefficients. However, the thickened coating made a coherent film when applied to uranium ore, and thus should be a better barrier.

Correlation of Permeability with Polymer Structure

In selection of coatings as radon barriers, it would be desirable to be able to predict the radon permeation coefficient based on the structure of the base polymer used in the coating. For this reason, we made some studies of possible relationships. Many chemical, morphological, and structural properties of the polymer can affect the permeability of a polymer.[14,16-18] These include chemical properties such as cohesive energy density (CED) and hydrogen bonding, morphological properties such as crystallinity and orientation, and the effect of structural groups in the polymer chain. It was quickly apparent that CED alone would not correlate with permeability, but we did find a reasonable correlation of the product of CED and polymer density with argon permeability, as shown in Fig. 4. This correlation did not appear to hold with the higher molecular weight noble gases. We then tried linear regression analysis with a number

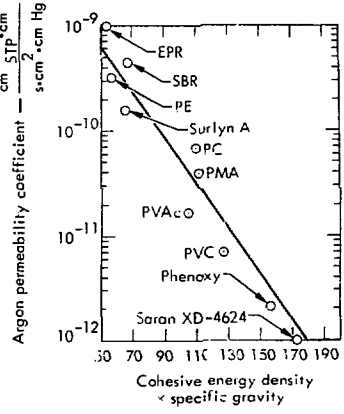

Fig. 4. Argon permeability coefficient vs cohesive energy density times specific gravity.

of polymer properties including CED, density, refractive index, gas molecular diameter (d), d^2, etc. The results were not particularly promising. We observed, however, that there was a correlation of the argon permeability of a number of polymers with the oxygen Permachor as developed by Salame[19] (see Fig. 5). This relationship was later extended to the other noble gases. Although Salame developed the Permachor equation empirically, he showed that there was a definite relationship to the classical relationship between permeability, diffusion, solubility, and temperature:

$$P = DS = (D_0 S_0) e^{-[(E_d + \Delta H)/RT]} \text{ (see Ref. 8).}$$

where

P = permeability coefficient

D = diffusion coefficient

S = solubility coefficient

E_d = energy of diffusion

ΔH = heat of solution of the gas in the polymer.

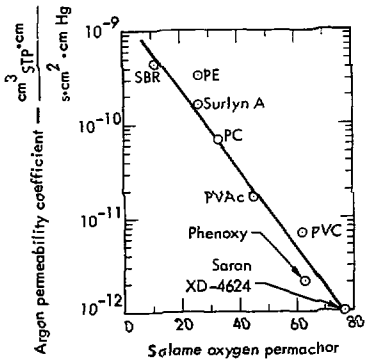

Fig. 5. Argon permeability coefficient vs Salame oxygen Permachor.

D_0 and S_0 are pre-exponential factors from the Arrhenius equations R is the gas constant and T is absolute temperature.

Salame's Permachor equation for the oxygen permeability of polymers at 25°C is: $P = (6.1 \times 10^{-9})e^{-0.115\,I}$, where I is the oxygen Permachor. The Permachor equation can also be written

$$P = e^{-0.115\,I}\,e^{-(11200/RT)},$$

which can be written in the form

$$P = e^{A+BI} \text{ or } \ln P = A + BI,$$

where A can be related to $(E_d + \Delta H)/RT$, and the coefficient B is determined by fitting experimental data.

We have studied the permeability of the noble gases, especially argon, krypton, and xenon, and have found that a relationship exists between the factors A and B and the square of the gas molecular diameters. Apparently it is possible to extrapolate to radon permeability through the determination of these relationships.

Because the data were limited to Ar, Kr, and Xe, a linear relationship was used. A least-squares fit was made of the oxygen Permachor to the permeability data we had determined for phenoxy, polyvinyl chloride, polycarbonate, polyethylene ionomer (Surlyn A), and Meares'[2,3] data for polyvinyl acetate. The coefficients A and B of the gases argon, krypton, and xenon thus obtained appeared to be linearly related to the d^2 of the gases. The least squares fit of this relationship resulted in the final equation

$$\ln(10^2 P) = (4.2354 + 0.4165\,d^2) + (0.088 - 0.0155\,d^2)I,$$

where P = permeability coefficient in $nm^2/Pa{\cdot}s$

d^2 = gas diameter squared, in $Å^2$

I = Salame's oxygen Permachor.*

Calculated values, using this equation, are shown in Table 4 along with our experimentally determined values for a number of polymers and coatings. The fit is quite good in most cases, but is rather poor for polyethylene. Because the Permachor is related to the structure of the polymer, this equation establishes a definite relationship to polymer structure and can be used to estimate the permeability of radon as well as the other noble gases through polymers.

There are relatively few permeability data in the literature for the noble gases as the major interest is in nitrogen, oxygen, carbon dioxide, and water as they may affect packaging of foods, etc. However, Burgess *et al*[20] have measured the permeability of polymethyl acrylate to argon and krypton and reported values equivalent to 1.3 and 0.75 $nm^2/Pa{\cdot}s$ at 20°C. The oxygen Permachor of polymethyl acrylate calculated from Salame's segmental values is 51. Using this value in the above equation, we calculate values for argon and krypton of 0.8 and 0.48 $nm^2/Pa{\cdot}s$, which agree to better than a factor of 2 with the experimentally determined values.

*Salame used the symbol π (pi) for Permachor. We use I to avoid confusion with the conventional use of π.

Table 4. Permeability coefficients of polymers calculated from Permachor.[a]

Material	Permachor (I)		Permeability, $nm^2/Pa \cdot s$				
			Ne	Ar	Kr	Xe	Rn
Phenoxy film	63	Experimental	1.9	0.20	0.08	0.016	–
		Calculated	2.0	0.27	0.12	0.02	0.0015
Polyvinyl chloride film, unplasticized	62		–	0.53	0.26	0.03	–
			2.1	0.29	0.14	0.02	0.0019
Polycarbonate film	33		–	4.1	3.8	1.5	1.4
			5.9	4.2	3.7	2.7	1.7
Surlyn A film	26		15	9.8	11	14	–
			7.6	7.8	8.1	8.5	9.1
Polyvinyl acetate (data of Meares)	45		15	1.1	0.36	–	–
			3.8	1.4	0.94	0.36	0.10
Epoxy, pigmented coating[b]	50		–	0.55	0.51	0.38	–
			3.2	0.88	0.53	0.16	0.03
Epoxy, unpigmented coating[c]	55		3.4	0.83	0.58	0.26	–
			2.7	0.56	0.30	0.07	0.001
Polyvinyl acetate,[d] plasticized coating	43		–	1.8	0.83	0.14	–
			4.1	1.7	1.2	0.50	0.16
Polyethylene film	26		–	25	34	60	113
			7	7.8	8.1	8.5	9.1
d^2, $Å^2$			8.0	11.6	13	16.4	20.9

[a] $\ln(10^2 P) = (4.2354 + 0.4166\, d^2) + (0.0880 - 0.0155\, d^2)\, I$

[b] Permachor estimated and arbitrarily lowered for pigment content.

[c] Permachor estimated.

[d] Permachor arbitrarily lowered for plasticizer content.

Permeability of Uranium Ore

The permeability was measured in a sample of uranium ore supplied by USBM. The ore sample was retrieved from the Dakota Mine located 29 miles northwest of Grants, New Mexico. The exact location within the mine was 657 ft from the portal. The change in sample permeability with confining pressure up to 800 psi was also measured. This pressure corresponds to approximately 800 ft of overburden.

Sample preparation was fairly standard. Several cored specimens were machined to the desired dimensions and attached to end adaptors for tubing connections. Confining oil pressure was exerted on a sample in both the radial and axial directions. Oil pressure was transmitted without penetration through a flexible plastic jacket cast around each sample. Steady state, axial flow of dry N_2 gas through the sample provided the conditions required for permeability determination.

The results of the measurements are summarized in Table 5.

Based on these measurements, ore permeability in the unconfined state ranges from 0.25 to 0.46 darcys, decreasing at most 25% at 800 psi confining pressure. Since the samples were oven dried at 50 to 60°C prior to the measurements, the above values represent the upper limit of permeability, and would be greatly reduced with the presence of interstitial water.

The permeability of rock is normally reported in darcys, but this can be converted into the units we have been using by introducing the appropriate gas viscosity value and the appropriate pressure correction. For argon gas, the viscosity is 222 x 10^{-6} poise (222 x 10^{-7} Pa•s). To convert darcys to [(cm^3•cm)/(s•cm^2•cm Hg)], divide darcys by about 1.7. To convert darcys to (nm^2/Pa•s), multiply darcys by 4.4 x 10^{10}. Thus, 0.25 darcy equals 0.15 [(cm^3•cm)/(s•cm^2•cm Hg)] or 1.1 x 10^{10} (nm^2/Pa•s).

TASK 3: EVALUATION OF TOXICITY OF COATINGS

Coatings suitable for use in a mine should be non-toxic during application, and the combustion and pyrolysis products should be of low toxicity. The volatile components of the coatings materials were identified qualitatively and semiqualitatively using gas chromatography and mass spectrography (GC/MS). The combustion and pyrolysis products were evaluated in two separate studies: (1) on cement-asbestos board specimens in the LLL-NBS Smoke Chamber, and (2) small scale pyrolysis studies of unsupported films of the coatings. Finally, toxicological evaluations were made of the data from these studies from published toxicological information; no animal toxicity studies were made.

Table 5. Permeability of uranium ore samples at 0 to 800 psi confining pressure.

Confining pressure, psig	Permeability, darcys		
	Sample 1	Sample 2	Sample 3
0	0.25	0.29	0.46
100	0.25	0.28	0.46
200	0.25	0.27	0.46
400	0.24	0.25	0.46
600	0.24	0.23	0.46
800	0.24	0.21	0.45

Smoke Chamber Studies of Coatings

Preparation of Specimens

The coatings were tested on cement-asbestos board substrates about 73 X 73 X 25 mm: the area exposed to heat and flame is about 65 X 65 mm. Thermocouples were imbedded at the center surface and at the lower surface, 6 mm from the lower edge. The lower thermocouple was impinged by the flame in the early tests (HydrEpoxy 300, Saran XD-7151, Essex polyester, and Ventron's Resitron II), but due to a slight modification of the smoke chamber, the thermocouple was slightly out of the flame area in the later tests. Some tests were also made on similar sized test specimens cut from uranium ore. There was no significant difference in the test results, and because use of uranium ore in the smoke chamber area required close monitoring by Hazard Control personnel (concern about release of alpha radiation), most tests were made on cement-asbestos board substrates only.

The coatings were prepared on the substrate usually by spraying, but sometimes by doctoring the coating material. It was usually necessary to use multiple coating to reach the desired coating thickness of 0.010 in. (0.25 mm). Although most coatings were tested at this thickness, the Resitron II coatings were 0.015 and 0.020 in. thick (0.38 and 0.51 mm), and the Hydro Seal coatings were only 0.007 and 0.008 in. thick (0.18 to 0.20 mm) and the Hydro Seal did not spread uniformly (did not wet) the previously dried coating.

Smoke Chamber Tests

This test studies the time dependence of toxic gas evolution under conditions designed to simulate a "fire" exposure. We used the LLL version of the NBS-developed Smoke Density Chamber. The procedure is given in NBS Technical Note 708 and was also desribed in the literature.[21]

In this test, the specimen is exposed to a radiant heat flux of 2.5 W/cm^2, (a) without the presence of an igniting flame (NF in tables and figures), and (b) in the presence of a small igniting flame (F in tables and figures). The radiant heat flux of 2.5 W/cm^2 is equivalent to that emitted by a black body at a temperature of 527°C (980°F). This is considered to be a moderately severe fire exposure. The chamber is continually monitored for smoke density, CO, and CO_2 content. The LLL chamber is also fitted with a continuous sampling device to measure HCℓ: this was used in the case of the Saran XD-7151 coatings tests. The results, however, were lower than expected, based on the results of our small scale pyrolysis tests. We now believe these HCℓ values from the smoke chamber tests to be invalid; they are low due to absorption on the chamber walls and sampling tubes, as well as incomplete recovery of HCℓ from the chamber gas.

The data from the smoke chamber tests are listed in detail in Table A-2 and Figs. A-1 to A-15 in Appendix A. The results may be summarized as follows:

1. HydrEpoxy 300, a water-based, pigmented epoxy coating. Under non-flaming conditions, the coating slowly produced a light smoke over a 30-min period, without any detectable production of CO or CO_2. Under flaming conditions, a light smoke was produced with an accompanying evolution of both CO (350 ppm) and CO_2 (1.4%). This amount of CO_2 is due to the pilot flame used under flame conditions. The quantities of these gases are similar to those found for other epoxy coatings previously tested in the same manner.
2. Saran XD-7151, a vinylidene chloride copolymer latex. Very little if any smoke was evolved from these coatings under either flaming or non-flaming conditions. No CO_2 was detected under non-flaming exposure. Under the flaming condition, the concentration of CO_2 reached about 1.4% in about 30 min, about the same as that for uncoated samples. We ascribe this to the combustion of the pilot flame. The Saran coating yielded 50 ppm CO in 25 min under a non-flaming condition and 300 to 500 ppm in 25 min under the flaming exposure. As indicated above, the HCℓ values are low.
3. Essex Polyester, a one-component (internally catalyzed, initiated by atmospheric moisture) styrenated polyester. This material slowly evolved a light smoke under the non-flaming exposure and a slightly denser smoke under the flaming exposure. Essentially no CO or

CO_2 was evolved under non-flaming exposure. In the flaming case a slow evolution of CO was observed with a maximum of 70 ppm in 30 min. Likewise a small amount of CO_2 was slowly evolved up to a maximum of 1.5% at 30 min; most of this can be ascribed to the pilot flame.

4. Resitron II, a catalyzed furfuryl alcohol polymer coating. This coating gave off no smoke under the non-flaming condition and a very light smoke under the flaming mode. Essentially no CO or CO_2 was evolved under non-flaming exposure. In the flaming mode, a slow evolution of CO was observed with a maximum of 100 ppm in 30 min. The CO_2 was evolved slowly up to a maximum of 1.5% at 30 min, most of which can be ascribed to the pilot flame.
5. WSU-118, a low viscosity modified epoxy developed for Bureau of Mines by Washington State University. The coating slowly evolved a dense smoke under non-flaming exposure; under flaming exposure a dense smoke was evolved moderately rapidly. No CO was detected under non-flaming exposure; under flaming exposure, a maximum of 300 ppm was evolved.
6. Aerospray 70, a polyvinyl acetate latex containing dibutyl phthalate plasticizer. Under both non-flaming and flaming exposure, the coating evolved a dense smoke moderately rapidly. No CO was detected under non-flaming exposure; under flaming exposure a maximum of 200 ppm was evolved.
7. EpiRez WD-510/EpiCure 872, a water-dispersed polyamine-cured epoxy coating. This was also evaluated cured with a blend of EpiCure 872 and 879; this cures harder and faster. Dense smoke evolved under both flaming and non-flaming conditions; evolution was slower under the non-flaming condition. No CO was detected under non-flaming condition; flaming exposure produced a maximum of 300 ppm.
8. Promulsion 200, an unidentified pigmented emulsion. This slowly produced a moderately dense smoke under non-flaming exposure; under flaming exposure it produced a somewhat denser smoke more rapidly. In the latter case transient ignition and flame extinction occurred throughout the test. No CO was detected under the non-flaming condition and only a minimal amount, 25 ppm, was detected under flaming exposure.
9. Hydro Seal, a water-based acrylic sealer, unpigmented. This slowly produced a moderate smoke in the non-flaming mode; in the flaming condition no ignition occurred, although a slightly denser smoke was produced, and a bit more rapidly. No CO was detected under either condition.

Smoke density curves, the specific optical density versus time, for several of the coatings are plotted in Fig. 6. Resitron II evolved a very light smoke and its specific optical density did not reach the value of 16, which is considered severe visual obscuration for a firefighter wearing a mask or other protective equipment. HydrEpoxy 300 produced a light smoke, with little difference on the transite substrate under flaming (F) or non-flaming (NF) conditions. Essex Polyester, also a light smoker, produced a slightly denser smoke more rapidly in the flaming mode. The EpiRez WD-510/EpiCure 872 coating evolved a dense smoke rapidly, especially in the flaming mode.

Flash Points of Coatings

Coatings materials for use in mines must have relatively high flash points to avoid danger of fire and explosion during application. The seven coatings selected for detailed evaluation were tested for flash point by the closed cup method (ASTM D-56). These coatings were: Acme's HydrEpoxy 300, Dow's Saran XD-7151, Ventron's Resitron II, Essex's styrenated polyester, Bureau of Mine's WSU-118, Cyanamid's Aerospray 70, and Celanese's EpiRez WD-510/EpiCure 872. Except for Essex's styrenated polyester, none of the coatings systems had a measurable flash point under the conditions of the test, i.e. less than 79°C (175°F).

The Essex Polyester had a closed cup flash point (ASTM D-56) of 20°C (68°F), and an open cup flash

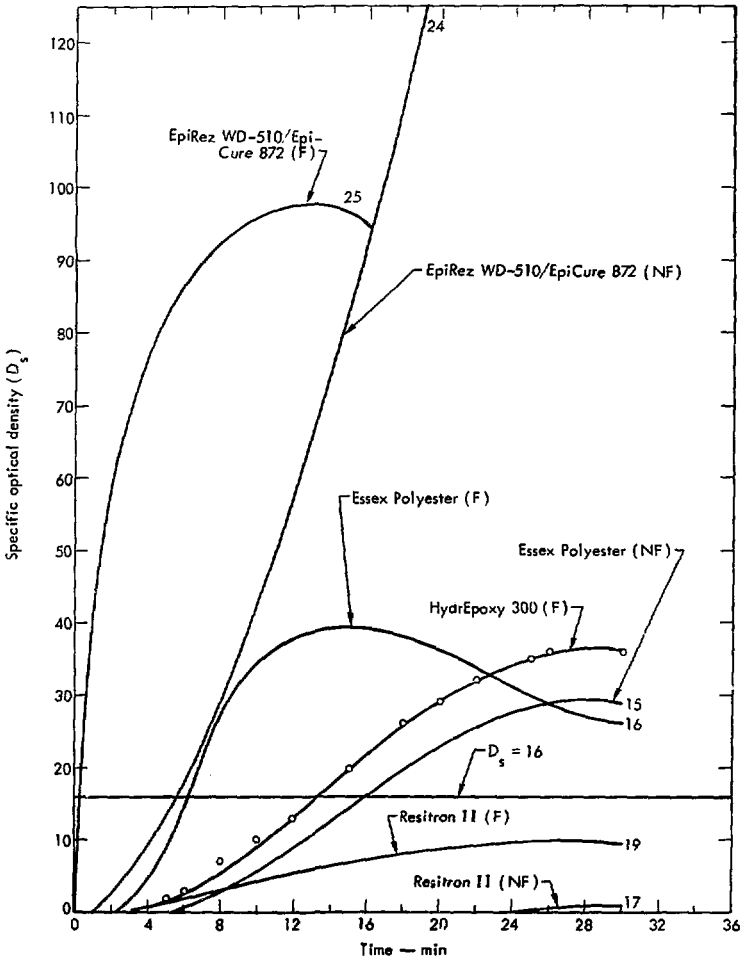

Fig 6. Smoke density curves for some representative coatings.

point (ASTM D-1310) of 39°C (102°F). This latter value is somewhat higher than the literature value[22] for styrene of 31°C, but may be due to the fact that the material tends to "skin over" rapidly, so must be stirred occasionally during the test.

Laboratory Pyrolysis Test Under Non-Flaming Conditions

In this section the pyrolysis data for seven selected polymer systems are summarized. It should be noted that our objectives were to determine in a semi-qualitative way the extent of toxic gas evolution and to compare the results for the different polymer systems.

The gas concentration data were obtained from small-scale laboratory experiments under non-flaming conditions. Samples, weighing between 25 and 75 mg, were isothermally heated in closed quartz tubes with a free volume of about 0.13 litre. The samples were pyrolyzed in normal laboratory air* at temperatures ranging from 200 to 600°C. Reaction times varied between 0.25 and 4 h. The longer reaction times were used at temperatures below 300°C to achieve a measurable degree of degradation. For each polymer system at least nine separate pyrolysis tests were made. In each test the experimental variables (time, temperature, and initial weight and/or film surface area of the sample) were varied to sample the infinite population of measurements.

At the completion of each pyrolysis experiment the gases were analyzed by mass spectroscopy (MS). For the Saran polymer two identical pyrolysis tests were done: one to obtain the gas analysis by MS; the second for the analysis of HCℓ. Hydrochloric acid was determined by dissolving the gaseous and absorbed HCℓ with dilute base followed by titration of the chloride ion. Selected gas mixtures, which were previously analyzed by MS, were also analyzed by gas chromatography (GC) to detect low level pyrolysis products. Standard gas mixtures containing CH_4, C_2H_6, and CO_2 were used to calibrate the chromatograph. The CO concentration is accurately determined by MS. Worst condition detection limit is about 0.3%. With a thermal conductivity detector the limit of detection for these gases was about 75 ppm. The results of the GC work (1) verified the presence and approximate concentration of the gases as measured by MS and, (2) showed that no other components were present at concentrations above 75 ppm.

Results and Discussion

This discussion will be mainly concerned with three topics: (1) HCℓ production from Saran; (2) Comparison of polymer stability and gas evolution data; (3) Comparison of CO evolution data from laboratory and smoke chamber tests.

HCℓ Production from Saran – It has previously been pointed out that the analytical system for determining HCℓ during smoke chamber tests is unreliable. In these tests most of the HCℓ appears to have been lost by adsorption on smoke particles or by dissolution in water vapor. Thus, the HCℓ data from the small scale laboratory tests (Table 1) are the only reliable data that can be used to predict the evolution of this gas. These data indicate that the HCℓ evolution is essentially time-dependent after 15 min and temperature-independent between 300 and 800°C. The best value appears to be the average of the 11 runs made under these conditions which is 0.26 ± 0.07 cm^3_{STP} HCℓ (gas) per mg of sample weight.

Comparison of Polymer Stability and Gas Evolution Data – In Fig. 7 the percent weight loss is plotted as a function of temperature for each polymer system. The use of somewhat longer reaction times at temperatures below 300°C relative to the reaction times used at the higher temperature distorts the plot somewhat. In effect the low temperature degradation is weighted more than the degradation at the higher temperature. However, at each temperature the data are comparable. Figure 7 clearly shows that Ventron's Resitron II, Essex Polyester, and HydrEpoxy 300 have significantly better thermal stability than the other polymer systems.

The evolved CO and CO_2 gas volumes as function of pyrolysis temperature are presented in Figs. A-16

*The tubes were filled with air at atmospheric pressure; the relative humidity was about 40-50%.

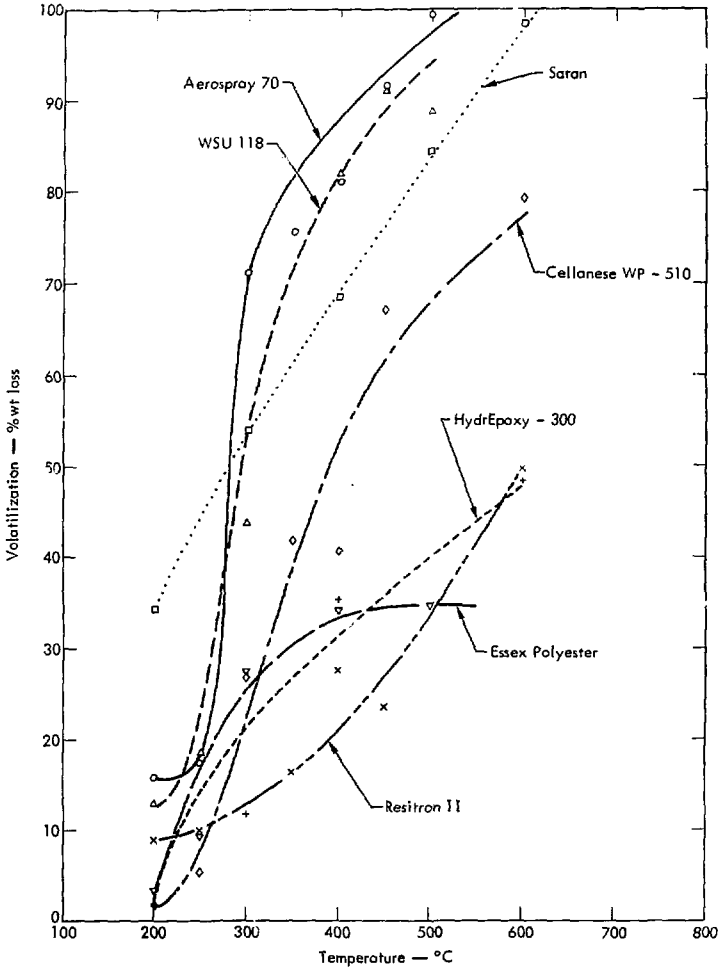

Fig. 7. Weight loss vs temperature.

and A-17, respectively.* A generalized CO evolution is shown in Fig. 8. The CO evolution for most coatings falls within the band. The Essex Polyester and Resitron show much different behavior. The gas volumes have been normalized to the initial sample weight (W_0). Under isothermal conditions, and in the presence of oxygen, the effect of increasing the reaction time is to decrease the CO production rate. In the case of Saran, where the largest number of data points were obtained, it appears that the CO evolution rate decreases as $t^{1/2}$. This is consistent with a rate controlled by a diffusion process. Our samples were films of nonuniform thickness, but generally of thickness larger than 10 mils. It is not unreasonable to postulate that the diffusion of oxygen into the film is the rate-controlling step, and that the reaction products (CO and CO_2) must diffuse out of the film. Figures 7 and A-16 also indicate that the gas evolution has an exponential temperature dependence. These facts lead us to postulate the following reaction rate expression for relatively thick Saran films:

$$\frac{dC_{CO}}{dt} = Ke^{-E_a/RT}\rho\frac{A}{L}t^{-1/2} ,$$

where K = Constant
E_a = The apparent activation energy
T = Temperature in K
A = Surface area of the film
L = Film thickness
R = Gas constant
ρ = Film density .

Similar rate expressions can be fitted to the other polymer systems.

Of principal interest in this study is the evolution of the highly toxic gas, carbon monoxide. Other potentially harmful gases, such as hydrocarbons and hydrogen, were also produced but at significantly lower levels. Based on the slopes of the CO-evolution curves (Fig. A-16) in the 300 to 500°C temperature interval the seven polymers are ranked as follows:

Best: Ventron's Resitron
Essex Polyester
HydrEpoxy 300
Saran (considering the HCℓ data in addition to the CO data)
Aerospray 70
WSU-118
EpiRez WD-510/EpiCure 872

These results are in general agreement with our conclusions obtained from the thermal stability data (Fig. 7).

For the degradation below 300°C this ranking may not be quite correct. Materials with low activation energies, such as Ventron's Resitron II and Essex Polyester, produce relatively more CO at these low temperatures than the other polymers.

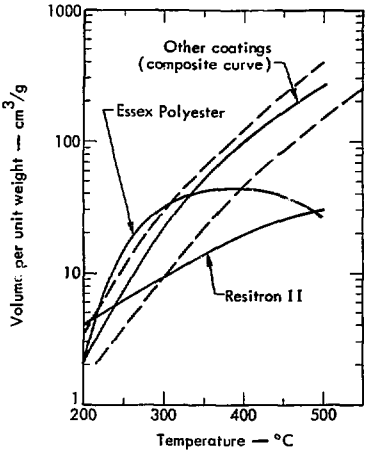

Fig. 8. Carbon monoxide evolution.

*Data obtained from runs above 500°C have been omitted from these graphs because in nearly all cases the oxygen depletion was near 100%. Under this condition the combustion mechanism must be expected to differ from the condition with high oxygen concentration.

Comparison of CO Gas Evolution Data from Laboratory and Smoke Chamber Tests – Smoke chamber tests were conducted under both flaming and non-flaming conditions. In the latter situation only the thermal flux from the heater produces the polymer degradation. This situation is comparable to the small-scale laboratory tests. In contrast to the laboratory tests, no CO was detected in the smoke chamber studies (non-flaming mode), except for Saran (~50 ppm).

In an attempt to predict the CO concentration from the laboratory tests we make the following assumptions:

a) The average temperature of the polymer film was either 300°C or 250°C for 0.5 h.
b) The film was uniformly heated (no flame).
c) The film thickness was uniform in both test situations and equal to 0.025 cm (10 mil).

These assumptions are expected to yield results that are upper limits for the predicted CO concentrations.*

The formula used to make these predictions is:

$$CO_{SC}(\text{ppm}) = 10^6 \times \frac{V_L^{CO}}{V_{SC}} \times \frac{A_{SC}}{A_L} \times \frac{t_{SC}}{t_L},$$

where

CO_{SC} = predicted CO concentration in the smoke chamber (SC)
V_L^{CO} = volume of CO (cm^3_{STP}) measured in laboratory test (L) at 300°C or 250°C
A = film surface area
t = reaction time.

The laboratory data was taken from Tables A-2 through A-8; A_{SC} = 42 cm^2; $V_{SC} \sim 5 \times 10^5$ cm^3, t_{SC} = 0.5 h. The predicted CO concentrations, based on the 250°C and 300°C laboratory results are summarized in Table 6.

The predicted CO concentrations are below the minimum detectable level of the CO analyzer on the smoke chamber (25 ppm).

*For example, thermocouple measurements indicate that the film surface reaches about 300°C after 0.5 h. For most of the time the film surface is at a lower temperature where the degradation is proceeding at a slower rate.

Comparisons between laboratory tests and the flaming smoke chamber tests are probably not valid. The degradation mechanisms are expected to differ considerably as is evident from the observed CO concentrations (~300 ppm).

GC/MS Analysis of Volatiles from Polymers

This section summarizes the analysis of the headspace volatiles from the seven selected polymer systems. In the case of two-component systems, each component was analyzed separately. Analysis was done using a computer automated gas chromatography/mass spectrometer (GC/MS) system. Initially, we attempted to identify the volatiles using only gas chromatography. This was not successful mainly because the elution times were not sufficiently reproducible to be matched against listed or suspected compounds.

We then used the computer-automated GC/MS system to identify most of the volatiles. The experimental conditions were as follows:

Columns: 1. 3 m X 3 mm o.d. glass, packed with Poropak Q, 80 to 100 mesh.
2. 2.8 m X 3 mm o.d. glass, packed with 10% OV-3 on 80 to 100 mesh Chromosorb WAD.
Carrier gas: Helium: flowrate 8 to 12 cm^3/min.
Temperature program: 65 to 220°C at 10 or 15°C/min.
Split ratio: 70% to MS and 30% to the flame ionization detector (FID).
Injector temperature: 200°C.
Separator temperature: 150°C.
Mass range: 12 to 250 automatic mass units (amu).
Integration time: 15 or 20 ms/amu.

Samples of selected liquid polymers and curing agents were stored in glass bottles and sealed with septum caps. The volatiles from the polymers were allowed to equilibrate with the normal air in the containers for at least several hours. The headspace was sampled through the septum cap with a 5 cm^3 gas-tight syringe. The syringe and needle were heated to about 80°C and flushed three times with the headspace gas before withdrawing a sample. This procedure was adopted to minimize loss of material through adsorption on the internal

Table 6. Predicted maximum CO concentrations in the smoke chamber under non-flaming conditions.

Polymer	Reaction temperature	
	300°C CO (ppm)	250°C CCO ppm
Saran	11[a]	7
HydrEpoxy-300	7	3
Essex Polyester	32	5
Resitron	9	12
EpiCure	12	4
Aerospray 70	11	4
WSU-118	19	4

[a]This value is predicted from the 2-h experiment. From the 0.5-h experiment we would predict 37 ppm; i.e., a value reasonably in agreement with the measured value.

syringe surfaces. The gas sample was then injected into the gas chromatograph. As each component was detected by the FID, the mass spectrum was obtained under computer control by automatically initiating the mass scan near the top of the GC peak. Background spectra were manually taken between GC peaks. All samples were first analyzed on the Porapak Q column, which is suitable for the separation of relatively low molecular weight compounds (up to C-6 hydrocarbons). Subsequently we also used the OV-3 column to separate and detect compounds with molecular weights up to about 200 amu.

After we had tentatively identified some of the vapors by their characteristic mass spectrum we prepared calibration mixtures containing 1000 ppm (by volume) of these compounds in methanol. A 0.5-μ sample of this mixture was then injected to calibrate the FID response and to confirm the mass spectrometric identification. From the recorded GC peak area we calculated calibration factors that took into account the change in GC peak shape with increasing elution time. The calibration factors for both columns were averaged to estimate the concentrations of all identified compounds in the 5 cm^3 headspace samples. The results are summarized in Table A-10. A typical mass spectrum, which was obtained during analysis of the headspace sample from Saran XD-7151 Latex, is shown in Fig. 9. This compound was readily identified as vinylidene chloride.

Although we were informed that WSU-118H contained DMP-30 [tris(dimethylaminomethyl)phenol] and DETA (diethylenetriamine), these materials were not identified in the vapors.

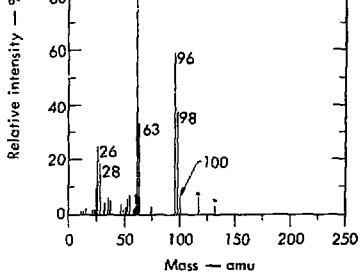

Fig. 9. Mass spectrum of vinylidene chloride from Saran latex (* = background peaks).

Toxicological Evaluation of Coatings

To evaluate the toxicity of the materials found by GC/MS in the study of the seven selected coatings, a table comparing the concentration found to the threshold limit value (TLV)* has been compiled (Table A-11 in Appendix A). The sample analyzed by GC/MS was collected from above the coating (or its components) in a closed container. Extrapolation of concentrations to a real mine situation is difficult. However, if one assumes these values are the maximum concentrations that can result from these coatings in a stagnant air situation, proper ventilation can be used to reduce them to a lower value where necessary. Most of the materials found in the coatings are innocuous with normal ventilation. However, because of the nature of one or more of the components of their curing vapors, the Saran XD-7151 latex and the WSU-118 coating must be handled carefully. The Saran coating liberates vinylidene chloride (suspect carcinogen) and the WSU-118 liberates vinyl chloride (carcinogen) and epichlorohydrin (sensitizer).

The smoke and pyrolysis vapors appear to contain little of toxicological significance other than CO and HCℓ: the latter is present only on pyrolysis of the Saran latex coating. The amount of CO generated would probably be small compared to that evolved from the other fire components, i.e., burning wood, diesel oil, or other waste materials. Possible "worst condition" calculations have been made as follows:

CO concentration in mine shaft:

Calculation conditions:

Mine ventilation rate = 100 ft/min.

Mine dimensions = 8 ft/8 ft

Film area liberating CO = 32 ft^2.

Volume of air moved through CO source = 6400 ft^3/min.

CO liberation rate = 400 × 550 ppm/ft^2/ft^3 in 30 min or 7320 ppm/ft^2/ft^3 in 1 min.

Calculation: (32 ft^2)(7320 ppm/ft^2/ft^3) (1/6400 ft^3) = 36.6 ppm CO average concentration/min.

This calculation was made for the Saran coating under flaming conditions and under very poor ventilation conditions. The Saran coating gave the highest CO concentration in the smoke chamber. Under these conditions the calculated CO concentration is close to the TLV for CO which is 50 ppm. Under more normal ventilation conditions, the CO concentration would be much lower.

HCℓ concentration in mine shaft:

Using the data in Table A-4 and assuming: (1) a 10-mil (0.254 mm) coating of the Saran XD-7151, (2) an 8 × 8 ft mine cross section, (3) a minimum air flow of 250 ft/min, and (4) that the coating reaches 400°C with adequate oxygen, we calculate that the pyrolysis of about 1/3 ft^2 per min of the coating would exceed the 10 ppm level. Even 5 ppm of HCℓ is highly irritating and may be the maximum allowable working level.

*Threshold limit values refer to airborne concentrations of substances and represent conditions under which it is believed that nearly all workers may be repeatedly exposed day after day without adverse effect. Because of wide variation in individual susceptibility, however, a small percentage of workers may experience discomfort from some substances at concentrations at or below the threshold limit, a smaller percentage may be affected more seriously by aggravation of pre-existing conditions or by development of an occupational illness.

References

1. R.L. Rock and D. K. Walker, Controlling Employee Exposure to Alpha Radiation in Underground Uranium Mines (Bureau of Mines, U.S. Dept. of the Interior, 1970).
2. P. Meares, J. Am. Chem Soc. 76, 3415 (1954).
3. P. Meares, Trans. Faraday Soc. 53, 101 (1957).
4. R.A. Pasternak, J.F. Schimsheimer, and J. Heller, J. Poly. Sci. 8, 467 (1970).
5. D.R. Paul and A.T. DiBenedetto, J. Poly. Sci., Part C, No. 10, 17-44 (1965).
6. R.J. Bearman, J. Phys. Chem., 61, 708-713 (1957).
7. R.M. Barber and H.T. Chio, J. Poly. Sci., Part C, No. 10, 111-138 (1965).
8. J. Crank and G.S. Park, Diffusion in Polymers (Academic Press, London and New York, 1968).
9. G.J. Van Amerongen, J. Poly. Sci. 5, 307 (1950).
10. G.J. Van Amerongen, Rubber Chemistry and Technology 37, 1065 (1964).
11. A.S. Michaels and H.J. Bixler, J. Poly. Sci. 50, 393 (1961).
12. A. Aitken and R.M. Barrer, Trans. Faraday Soc. 51, 116 (1955).
13. R.M. Barrer and G. Skirrow, J. Poly. Sci. 3, 549 (1948).
14. H.J. Bixler, A.S. Michaels, and M. Salame, J. Poly. Sci. A, 1, 895 (1963).
15. I. Sobiolev, J.A. Meyer, V. Stannett, and M. Szwarc, J. Poly. Sci. 17, 417 (1955).
16. A.S. Michaels and H.J. Bixler, J. Poly. Sci. 50, 293 (1961).
17. A.S. Michaels and H.J. Bixler, J. Poly. Sci. 50, 413 (1961).
18. H. Alter, J. Poly. Sci. 57, 925 (1962).
19. M. Salame, Polymer Division Preprints, American Chemical Society 8, No. 1 (1967).
20. W.H. Burgee, H.B. Hopfenberg, and V.T. Stannett, J. Macromol. Sci.-Phys., B5(1), 23-40 (1971).
21. J.R. Gaskill, Jour. Fire and Flammability 1, 183-216 (1970).
22. R.H. Boundy and R.F. Boyer, Styrene, Its Polymers, Copolymers, and Derivatives (Hafner Publishing Co., New York and London, 1952) p. 744.

Appendix A:

Tables and Figures

Table A-1. Permeation coefficients of supported coatings.[a]

Maker, Name	Type	Gas	Permeation coefficient of coating	
			$\frac{cm^3_{STP} \cdot cm}{s \cdot cm^2 \cdot cm\ Hg}$	$\frac{nm^2}{Pa \cdot s}$
Acme, HydrEpoxy 300	Pigmented, water-dispersed Epoxy	Ar	6.7×10^{-11}	5.0
Acme, HydrEpoxy 300 Mod 1	Pigmented, water-dispersed Epoxy	Ar	1.4×10^{-11}	1.1
Acme, HydrEpoxy 300 Mod 2	Pigmented, water-dispersed Epoxy	Ar	7.3×10^{-12}	0.55
Acme, HydrEpoxy 300 Mod 2	Pigmented, water-dispersed Epoxy	Kr	6.8×10^{-12}	0.51
Acme, HydrEpoxy 300 Mod 2	Pigmented, water-dispersed Epoxy	Xe	5.0×10^{-12}	0.38
		(Rn)[b]	(4×10^{-12})	(0.3)
Acme, HydrEpoxy 156/300[c]	Pigmented, water-dispersed Epoxy	Ar	1.7×10^{-11}	1.3
Acme, HydrEpoxy 156/300	Pigmented, water-dispersed Epoxy	Kr	1.4×10^{-11}	1.1
Acme, HydrEpoxy 156/300	Pigmented, water-dispersed Epoxy	Xe	1.4×10^{-11}	1.1
		(Rn)	(1.3×10^{-11})	(1)
Am. Cyanamid, Aerospray 52	Alkyd resin dispersion	Ar	1.1×10^{-11}	0.83
Am. Cyanamid, Aerospray 70	Plasticized polyvinyl acetate emulsion	Ar	2.4×10^{-11}	1.8
Am. Cyanamid, Aerospray 70	Plasticized polyvinyl acetate emulsion	Kr	1.1×10^{-11}	0.83
Am. Cyanamid, Aerospray 70	Plasticized polyvinyl acetate emulsion	Xe	1.9×10^{-12}	0.14
		(Rn)	(4×10^{-13})	(0.03)
Celanese, EpiRez WD-510/EpiCure 879/EpiCure 872	Non-pigmented, water-dispersed epoxy	Ar	8.7×10^{-12}	0.65
Celanese, EpiRez WE-3520/EpiCure BCT-60-8533	Non-pigmented, water-dispersed epoxy	Ne	4.5×10^{-11}	3.4
Celanese, EpiRez WE-3520/EpiCure BCT-60-8533	Non-pigmented, water-dispersed epoxy	Ar	1.1×10^{-11}	0.83
Celanese, EpiRez WE-3520/EpiCure BCT-60-8533	Non-pigmented, water-dispersed epoxy	Kr	7.7×10^{-12}	0.58
Celanese, EpiRez WE-3520/EpiCure BCT-60-8533	Non-pigmented, water-dispersed epoxy	Xe	3.5×10^{-12}	0.26
		(Rn)	1.1×10^{-12}	0.083
Dow, Saran XD-4624	Vinylidene chloride copolymer latex	Ar	4.4×10^{-13}	0.033
Dow, Saran XD-4624	Vinylidene chloride copolymer latex	Kr	2.2×10^{-13}	0.017
Dow, Saran XD-4624	Vinylidene chloride copolymer latex	Xe	8.9×10^{-14}	0.0067
		(Rn)	1.8×10^{-14}	0.0014

Table A-1. Permeation coefficients of supported coatings (continued).

Maker, Name	Type	Gas	Permeation coefficient of coating	
			$\frac{cm^3_{STP} \cdot cm}{s \cdot cm^2 \cdot cm\ Hg}$	$\frac{nm^2}{Pa \cdot s}$
Dow, Saran XD-7151	Vinylidene chloride copolymer latex	Ar	2.0×10^{-13}	0.015
Dow, Saran XD-7828	Vinylidene chloride copolymer latex	Ar	2.7×10^{-13}	0.020
Dowell, M159/M171	Vinylidene chloride copolymer latex plus thickener	Ar	3.9×10^{-13}	0.029
Dowell, M175/M171	Vinylidene chloride copolymer latex plus thickener	Ar	7.6×10^{-13}	0.057
Essex, moisture curing unsaturated polyester	Pigmented styrenated polyester	Ar	1.7×10^{-10}	13.
Goodrich, Geon 660X1	Vinylidene chloride copolymer latex	Ar	4.9×10^{-12}	0.37
Goodrich, Geon 652	Vinylidene chloride copolymer latex	Ar	1.7×10^{-12}	0.13
Monsanto, Monflex 4500	Vinyl chloride copolymer latex	Ar	8.0×10^{-12}	0.60
Monsanto, Monflex 4514	Vinyl chloride copolymer latex	Ar	6.0×10^{-12}	0.45
Monsanto/Rohm and Haas, Monflex 4500/Rhoplex HA-20	Vinyl chloride copolymer latex/vinylidene chloride-acrylic copolymer latex	Ar	4.2×10^{-12}	0.32
Pan. Am. R&D, GPC-500	Acrylic solution	Ar	8.5×10^{-11}	6.4
Preserv-O-Paint, CP-5005	Epoxyized polyester urethane	Ar	2.9×10^{-11}	2.2
Rohm and Haas, Acryloid C-10 LV	Polymethyl acrylate solution	Ar	3.9×10^{-11}	2.9
Quaker, Quaker Coat		Ar	3.5×10^{-11}	2.6
Union Carbide, 9484-153-100	Acrylonitrile copolymer latex	Ar	1.0×10^{-10}	7.5
Ventron, Resitron II	Furan polymer	Ar	1.5×10^{-13}	0.011

[a] All coatings were applied on polyethylene ionomer, Surlyn A, about 0.05 mm, except Resitron II which was an unsupported film. Coefficients have been calculated for coating alone.

[b] Radon coefficients are estimated values obtained by extrapolating values of Ar, Kr, and Xe coefficients vs gas diameter squared.

[c] HydrEpoxy 300 (0.0025 mm) on top of HydrEpoxy 156 (0.0018 mm) on Surlyn A.

Table A-2. Smoke chamber evaluation of coatings on asbestos-cement board or uranium ore.
Light obscuration data

Test No.	Substrate	Coating	Exposure[a]	Specific optical density[b] at time, min 5	10	15	20	25	30	Maximum specific optical density	Obscuration time[c], min (1-16)	Gas concentrations, at time, min 5 CO	5 CO_2	10 CO	10 CO_2	15 CO	15 CO_2	20 CO	20 CO_2	25 CO	25 CO_2	30 CO	30 CO_2
GH-1	A-C Bd	None	NF	0	0	0	0			0	NR												
GH-2	A-C Bd	None	F	0	0	0	0			0	NR						0.5		0.8				
GH-3	A-C Bd	HydrEpoxy 300	NF	2	7	13	20	29	36	36	17.4												
GH-4	A-C Bd	HydrEpoxy 300	F	2	10	20	29	35	36	36	13.0			125	0.4	200	0.7	250	1.0	300	1.2		
GH-5	U Ore	None	F	0	0	2	2	2	2	2	NR							50	1.0				
GH-6	U Ore	None	NF	0	1	2	2	2	2	2	NR												
GH-7	U Ore	HydrEpoxy 300	F	3	16	37	50	50	44	51	9.9	50	0	150	0.4	200	0.7	250	0.9	300	1.2	350	1.4
GH-8	U Ore	HydrEpoxy 300	NF	0	4	11	17	22	30	30	18.9												
GH-9	A-C Bd	XD-7151	F	0	1	1	1	1	1	1	NR			150	0.4	175	0.7	250	0.8	270	1.1	320	1.2
GH-11	A-C Bd	XD-7151	NF	0	0	1	1	1	1	1	NR					25		40	0.1	30	0.1	50	0.1
GH-12	A-C Bd	XD-7151	F	0	1	1	2	2	2	2	NR	75	0.4	200	0.5	260	0.8	350	1.0	420	1.2	450	1.4
GH-13	U Ore	XD-7151	F	0	0	1	1	0	1	1	NR	100	0	250	0.3	300	0.5	500	0.6	500	1.0	550	1.2
GH-14	U Ore	XD-7151	NF	0	0	1	2	2	2	2	NR					50	0	60	0	60	0	100	0
GH-15	A-C Bd	Essex Polyester	NF	0	5	14	22	28	29	29	15.8											20	
GH-16	A-C Bd	Essex Polyester	F	11	34	39	36	30	26	39	6.0	20	0.2	30	0.5	50	0.8	50	1.1	60	1.2	70	1.5
GH-17	A-C Bd	Resitron II	NF	0	0	0	0	1	1	1	NR											20	
GH-18	A-C Bd	Resitron II	F	0	2	4	6	7	7	7	NR	20	0.2	40	0.3	50	0.5	80	0.9	90	1.1	100	1.5
GH-19	A-C Bd	Resitron II	F	2	4	7	8	9	9	10	NR	20	0.2	40	0.5	50	0.8	65	1.2	80	1.4	90	1.5
GH-20	A-C Bd	WSU-118	NF	10	25	54	77	92	102	102	7.2												
GH-21	A-C Bd	WSU-118	F	50	89	109	111			111	2.4							300					
GH-22	A-C Bd	Aerospray 70	NF	41	83	91	87			91	2.6												
GH-23	A-C Bd	Aerospray 70	F	55	87	87				88	2.3	100		180		200							
GH-24	A-C Bd	WD-510/872	NF	15	43	83	129	155	172	172	5.4												
GH-25	A-C Bd	WD-510/872	F	83	97	95				97	0.5	200		250		300							
GH-26	A-C Bd	WD-510/872/879	NF	17	27	48	57	64	76	76	4.7												
GH-27	A-C Bd	WD-510/872/879	F	59	119	147	147			150	3.2	150		250				300					
GH-28	A-C Bd	Promulsion 200	NF	5	26	50	71	84	89	89	7.7												
GH-29	A-C Bd	Promulsion 200	F	58	105	122				122	2.3					25							
GH-30	A-C Bd	Hydro Seal	NF	2	4	10	18	26	35	42	18.0												
GH-31	A-C Bd	Hydro Seal	F	7	34	52	58			58	6.8												

[a] NF = non flaming; F = flaming; NR = not reached.
[b] Specific optical density (D_s) = [(Volume of chamber)/(Area of emitting surface X length of optical path)] X $100 \log_{10}$ (100/transmission)
CO in ppm; CO_2 in %. CO_2 meter not functioning after GH-19. Lowest detectable limits: O_2 25 ppm, CO_2 0.1%
[c] Obscuration time = time to reach specific optical density of 16 (severe visual obscuration for fire fighter wearing mask)

Table A-3. Pyrolysis study of HydrEpoxy 300.

Sample wt, mg	Residue wt, mg	Wt loss, mg	Loss wt, %	Surface area, mm^2	Pyro temp, °C	Pyro time, h	Gas evolved, cm^3_{STP}				Gas evolved/sample wt, cm^3_{STP}/g				O_2 loss, %
							CO	CO_2	CH_4	C_2H_6	CO	CO_2	CH_4	C_2H_6	
25.244	23.909	1.335	5.3	166	200	16.0	0.18	0.38	~0	~0	7	15	~0	~0	4.3
25.476	23.742	1.734	6.8	133	200	29.5	0.50	0.53	~0	~0	20	21	~0	~0	7.8
25.348	22.337	3.011	11.9	139	300	2.0	0.42	1.08	~0	~0	17	43	~0	~0	10.4
24.633	20.150	4.483	18.2	133	300	16.0	1.13	2.28	0.02	~0	44	90	4	~0	37.2
25.400	16.360	9.040	35.6	132	400	2.0	2.29	6.24	0.02	~0	90	246	4	~0	41.1
25.354	18.234	7.120	28.	95	400	0.5	0.96	1.86	0.04	0.01	38	73	2	1	18.4
25.074	12.880	12.194	48.6	99	600	0.5	~0	11.6	~0	~0	~0	402	~0	~0	53.6
25.110	11.965	13.145	52.4	96	800	0.5	~0	12.7	~0	~0	~0	506	~0	~0	57.9

Table A-4. Pyrolysis study of Saran XD-7151 film
(95% Saran plus 5% polyvinyl alcohol solution).

Sample wt, mg	Residue wt, mg	Wt loss, mg	Loss wt, %	Surface area, mm^2	Pyro temp, °C	Pyro time, h	Gas evolved, cm^3_{STP}				Gas evolved/sample st, cm^3_{STP}/g				O_2 loss, %
							CO	CO_2	HCℓ	CH_4	CO	CO_2	HCℓ	CH_4	
50.448	48.380	2.068	4.1	106	150	3.0	∿0	0.07	0.57	∿0	∿0	1	11	∿0	5.6
49.232	32.270	16.962	34.5	104	200	2.0	0.13	0.11	7.14	∿0	3	2	15	∿0	∿0
25.501	11.883	13.618	53.4	55	300	0.25	0.24	0.24	5.26	0.01	10	10	21	1	0.2
25.074	11.205	13.869	55.3	56	300	0.5	0.35	0.50	5.05	0.04	14	20	202	2	1.5
24.924	12.175	12.749	51.2	57	300	1.0	0.44	0.47	5.43	∿0	18	19	215	∿0	1.5
25.143	11.538	13.605	54.1	62	300	2.0	0.32	0.50	5.85	∿0	13	20	233	∿0	3.1
24.550	9.550	15.000	61.1	56	400	0.25	0.76	0.80	7.45	∿0	31	33	304	∿0	0.8
24.410	10.195	14.215	58.2	47	400	0.5	0.95	1.43	8.28	∿0	39	58	330	∿0	8.6
25.352	9.450	14.902	58.9	56	400	1.0	1.09	1.66	6.57	0.03	43	66	259	1	8.6
25.290	8.120	17.170	67.9	55	400	2.0	1.42	3.08	5.45	∿0	56	122	215	∿0	16.9
25.053	7.385	17.668	70.5	48	400	4.0	1.92	3.19	7.97	0.04	77	127	318	2	20.9
24.3	8.819	15.481	63.7	74	400	0.25	1.55	3.65		0.08	64	150		3	20.5
74.9	23.474	51.426	68.7	148	400	0.75	7.35	7.95		0.59	98	106		8	45.9
24.4	.343	24.06	98.6	86	600	0.5	9.55	6.80		0.04	391	279		2	46.9
23.153	.336	22.817	98.5	83	600	0.5	8.55	6.15		∿0	382	266		∿0	64.5
49.69	∿0	49.69	100		600	0.5	18.85	8.70	(10.9)	0.06	379	175	219	1	76.0
23.1	∿0	23.1	100	82	800	0.75	0.62	14.6		∿0	27	632		∿0	39.5
22.2	∿0	22.2	100	82	800	0.25	3.14	10.9	(6.7)	∿0	141	491	302	∿0	46.3
75.1	13.77	61.32	81.7		800	0.25	13.14	13.4	(17.35)	∿0	178	178	231	∿0	81.0

Table A-5. Pyrolysis study of Essex Polyester.

Sample wt, mg	Residue wt, mg	Wt loss, mg	Loss wt, %	Surface area, mm^2	Pyro temp, °C	Pyro time, h	Gas evolved, cm^3_{STP}				Gas evolved/sample st, cm^3_{STP}/g				O_2 loss, %
							CO	CO_2	CH_4	H_2	CO	CO_2	CH_4	H_2	
49.793	48.069	1.724	3.5	117	200	4.0	∿0	1.05	∿0	∿0	∿0	21	∿0	∿0	10.5
25.631	23.109	2.522	9.8	42	250	4.5	0.24	0.65	∿0	0.04	9	25	∿0	2	2.9
75.200	62.600	12.600	16.8	105	300	1.0	1.42	3.49	0.03	0.08	19	46	1	1	20.4
50.654	36.710	13.944	27.5	104	300	2.0	1.57	4.81	0.04	0.09	31	95	1	2	23.5
25.583	17.641	7.942	31.0	56	350	2.6	1.09	3.10	∿0	0.07	43	121	∿0	3	13.6
49.292	32.340	16.952	34.3	104	400	1.0	2.13	10.58	0.04	0.20	43	215	1	4	45.3
49.322	32.631	16.691	33.8	108	450	1.5	∿0	15.52	0.08	0.25	—	315	2	5	60.2
25.678	16.792	8.886	34.6	52	500	0.5	0.71	7.95	0.13	0.17	28	310	5	7	32.4
25.070	16.402	8.668	34.6	56	500	1.5	0.52	8.33	0.01	∿0	21	332	1	∿0	34.8
74.828	48.971	25.857	34.6	105	600	0.5	7.06	19.39	0.72	1.63	94	259	10	22	98.3

Table A-6. Pyrolysis study of Ventron's Resitron II.

Sample wt, mg	Residue wt, mg	Wt loss, mg	Loss wt, %	Surface area, mm^2	Pyro temp, °C	Pyro time, h	Gas evolved, cm^3_{STP}				Gas evolved/sample st, cm^3_{STP}/g				O_2 loss, %
							CO	CO_2	CH_4	C_2H_6	CO	CO_2	CH_4	C_2H_6	
40.500	45.364	4.136	8.4	127	150	4.0	∿0	0.20	∿0	∿0	∿0	4	∿0	∿0	1.4
75.222	72.712	2.510	3.3	165	150	6.0	0.32	0.30	∿0	∿0	4	4	∿0	∿0	2.5
50.416	45.892	4.524	9.0	138	200	2.0	0.18	0.43	∿0	∿0	4	9	∿0	∿0	4.6
74.557	67.284	7.273	9.8	150	250	1.0	0.42	1.74	∿0	∿0	6	23	∿0	∿0	5.4
50.359	44.900	5.459	10.8	127	300	1.0	0.27	1.38	0.01	∿0	5	27	∿0	∿0	4.3
25.506	21.300	4.206	16.5	56	350	1.0	0.38	0.83	0.05	∿0	15	32	2	∿0	2.6
25.314	18.312	7.002	27.7	25	400	0.5	0.45	1.23	0.07	∿0	18	49	3	∿0	6.4
75.178	57.403	17.775	23.6	138	450	0.25	1.56	3.87	0.44	0.08	21	51	6	1	14.2
25.165	12.650	12.515	49.7	27	600	0.5	0.85	14.61	∿0	∿0	34	581	∿0	∿0	74.2

Table A-7. Pyrolysis study of Aerospray 70.

Sample wt, mg	Residue wt, mg	Wt loss, mg	Loss wt, %	Surface area, mm^2	Pyro temp, °C	Pyro time, h	Gas evolved, cm^3_{STP}				Gas evolved/sample st, cm^3_{STP}/g				O_2 loss, %
							CO	CO_2	CH_4	H_2	CO	CO_2	CH_4	H_2	
75.602	63.423	12.179	16.1	195	200	4.0	0.14	0.52	~0	0.06	2	7	~0	1	2.7
75.043	62.042	13.001	17.3	163	250	3.0	.50	1.25	0.04	~0	7	17	1	~0	10.8
51.001	14.709	36.392	71.4	144	300	3.0	1.12	2.58	.18	~0	22	50	4	~0	20.0
50.326	12.197	38.129	75.8	98	350	2.0	1.97	4.09	0.10	0.07	39	80	2	1	28.3
50.550	9.554	40.996	81.1	154	400	3.0	4.52	13.01	0.28	0.16	90	257	6	3	88.5
74.905	6.953	67.952	90.7	175	450	1.75	8.36	17.39	0.84	0.35	112	230	10	5	99.1
25.673	0.155	25.518	99.4	55	500	1.0	7.01	14.30	0.74	0.36	273	557	29	14	71.8
25.452	0.086	25.366	99.7	42	550	1.0	6.53	13.52	0.61	0.30	256	531	24	12	83.9
25.494	0.412	25.082	98.4	46	600	0.5	4.80	20.96	0.09	0.10	188	822	4	4	88.0

Table A-8. Pyrolysis study of EpiRez WD-510/EpiCure 872

Sample wt. mg	Residue wt. mg	Wt loss, mg	Loss wt. %	Surface area, mm^2	Pyro temp. °C	Pyro time, h	Gas evolved, cm^3_{STP}				Gas evolved sample st. cm^3_{STP} g				O_2 loss, %
							CO	CO_2	CH_4	H_2	CO	CO_2	CH_4	H_2	
74.584	73.091	1.473	2.0	84	200	4.0	0.18	0.30	0.06	~0	3	4	1	~0	2.8
75.405	71.345	4.06	5.4	99	250	3.0	0.27	0.79	0.06	~0	4	10	1	~0	8.3
49.791	36.452	13.339	26.8	81	300	3.0	0.71	1.43	0.08	~0	14	29	2	~0	14.9
51.707	29.963	21.744	42.1	41	350	2.0	2.18	3.79	0.24	0.06	52	90	6	1	50.6
50.534	30.0	20.534	40.6	72	400	2.5	5.78	8.94	0.24	0.04	114	177	5	1	73.9
24.715	8.1	16.615	67.2	64	450	1.5	8.54	9.17	0.31	0.03	346	371	13	1	61.2
25.314	4.0	21.314	84.2	72	500	1.0	10.22	10.04	0.47	0.22	404	397	19	9	72.7
75.326	35.4	39.926	53.0	55	550	1.0	17.36	7.73	4.53	0.51	231	103	60	7	99.1
25.700	5.3	20.40	79.4	20	600	0.5	5.27	19.63	0.06	0.22	205	764	2	9	99.4

Table A-9. Pyrolysis study of WSU 118 (5.3 parts R, 1.0 parts H).

Sample wt, mg	Residue wt, mg	Wt loss, mg	Loss wt, %	Surface area, mm^2	Pyro temp, °C	Pyro time, h	Gas evolved, cm^3_{STP}				Gas evolved/sample st, cm^3_{STP}/g				O_2 loss, %
							CO	CO_2	CH_4	H_2	CO	CO_2	CH_4	H_2	
75.412	65.578	9.894	13.1	63	200	4	0.17	0.26	~0	~0	2	3	~0	~0	6.9
75.340	61.744	13.596	18.05	95	250	3	0.28	0.39	~0	~0	4	5	~0	~0	7.7
50.379	28.262	22.117	43.9	70	300	3	0.97	2.12	0.06	~0	19	42	1	~0	37.6
50.632	--	--	--	39	350	2	2.71	6.22	0.13	~0	54	123	3	~0	57.7
49.492	8.989	40.503	81.8	48	400	2.5	6.23	11.28	0.17	0.07	126	228	3	1	80.7
25.668	2.079	23.589	91.9	18	450	1.5	5.74	10.21	0.13	0.08	224	398	5	3	71.9
25.012	2.686	22.326	89.3	23	500	1.25	7.33	12.69	0.23	0.13	293	507	9	1	83.9
74.927	10.170	64.757	86.4	55	550	1	15.44	8.71	3.46	0.64	206	116	46	8	98.6
25.805	2.056	23.749	92.0	45	600	0.5	7.76	15.76	0.11	0.33	301	611	4	13	99.4

Table A-10. TLV of organic materials released during curing of several radon barrier coatings.

Coating	Compound	Volume found, ppm	TLV, ppm	Personal guess, ppm
EpiRez WD-510	Acetone	25-49	1000	
	MEK	10-24	200	
	Butanol	10-24	100	
	Toluene	10-24	100	
	Xylene	0-9	100	
	2-Ethoxy ethylacetate	10-24	100	
	2-Methyl butanol	100-199	--	100
EpiCure 872	Ethylene	10-24	1000	
	Propane	0-9	1000	
	Vinyl Acetate	10-24	10	
	Toluene	10-24	100	
	Xylene	10-24	100	
	Ethyl benzene	200-399	100	
Resitron II (Resin)	Methanol	0-9	200	
	2-Methyl furan	0-9	--	10
	Vinyl acetate	0-9	10	
	MEK	0-9	200	
	Acetone	25-49	1000	
	Furfural	25-49	5	
	Furfuryl alcohol	200-399	5	
Aerospray 70	Acetaldehyde	0-9	100	
	Ethanol	0-9	1000	
	Vinyl acetate	200-399	10	
	Acetone	400-699	1000	
HydrEpoxy 300 (A component)	Ethylene	25-49	1000	
	Acetone	10-24	1000	
	Vinyl acetate	25-49	10	
HydrEpoxy 300 (B component)	Acetone	0-9	1000	
	Vinyl acetate	0-9	10	
Saran XD-7151 Latex	2-Methyl propene	0-9	--	200
	Butanol	0-9	100	
	2-Methyl-2-propanol	25-49	100	
	Butyl acrylate	50-99	--	10-100
	Vinylidene chloride	100-199	--	1-10
	Acetone	200-399	1000	
	Acrylonitrile	20-399	20	

Table A-10. TLV of organic materials released during curing of several radon barrier coatings (continued).

Coating	Compound	Volume found, ppm	TLV, ppm	Personal guess, ppm
Essex Polyester (fresh[a])	MEK	25-49	200	
	Styrene	200-399	100	
	Toluene	400-699	100	
	Acetone	10,000 +	1000	
Essex Polyester (after 48 h[b])	Ethylene chloride	10-24	50	
	MEK	25-49	200	
	Styrene	700-999	100	
	Acetone	> 20,000	1000	
Essex Polyester (after curing total gas)	Toluene	10-24	100	
	Propyl heptanol	200-399	—	10-100
	Ethyl benzene	400-699	100	
	Xylene	700-999	100	
	Benzene	1000-2499	25	
	Isopropyl benzene	1000-2499	50	
	Acetone	2500-10,000	1000	
Essex Polyester (vapor over cured material)	Benzene	10-24	25	
	Benzaldehyde	50-99	—	10-100
	Acetone	200-399	1000	
WSU-118 (R component[a])	Vinyl chloride	25-49	1	
	Ethylene chloride	50-99	50	
	Epichlorohydrin	50-99	5	
	Acetone	100-199	1000	
WSU-118 (H component[a])	Trimethylamine	200-399	—	10
	Toluene	400-699	100	
	Dimethylamine	1000-2499	10	
	A[c]		—	?
	B[c]		—	?

[a] Poropak Q column only: To check styrene content in fresh material.

[b] Stabilized styrene: different elution time.

[c] Unresolved compound: excludes, DMP-30, DETA.

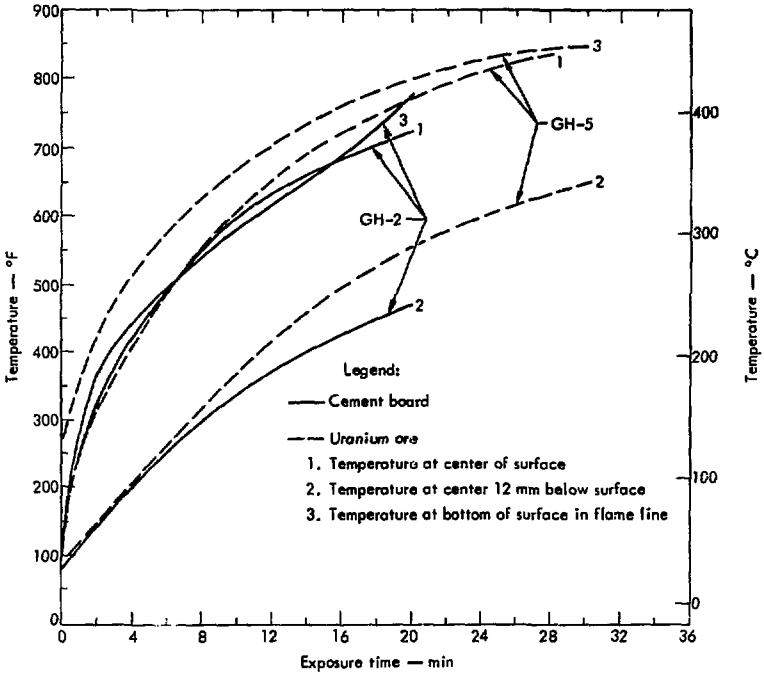

Fig. A-1. Surface and body temperatues of uncoated cement-board and uranium-ore squares exposed to 2.5 W/cm^2 radiant heat with pilot flame.

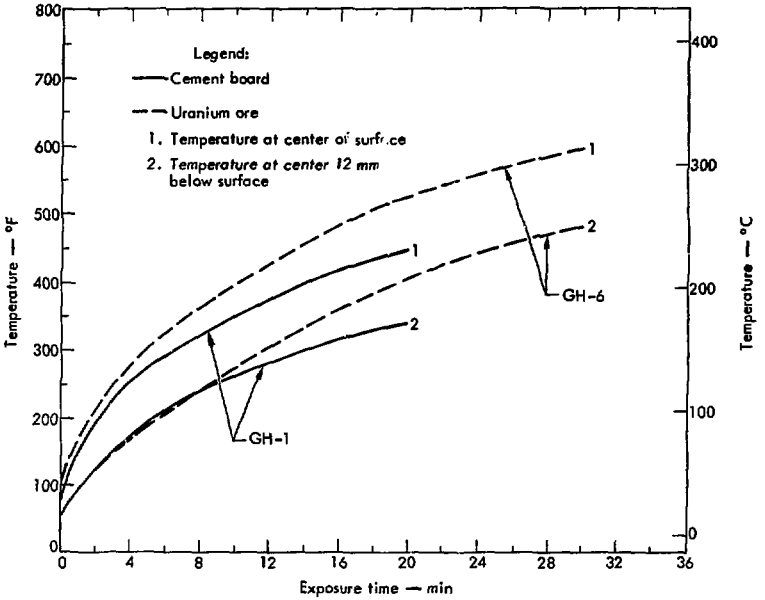

Fig. A-2. Surface and body temperatures of uncoated cement-board and uranium-ore squares exposed to 2.5 W/cm^2 radiant heat, without pilot flame.

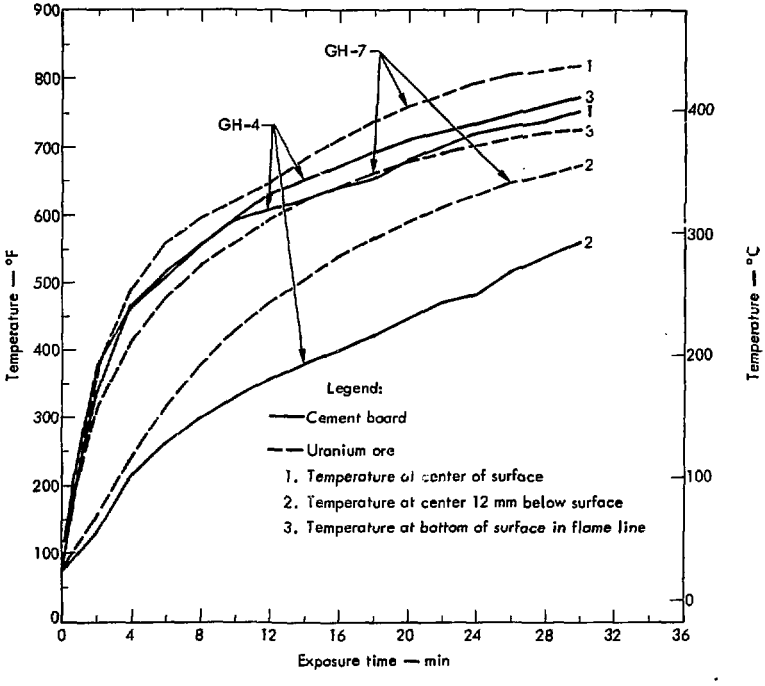

Fig. A-3. Surface and body temperature of cement-board and uranium-ore squares whose front surface had been coated with 10 mils of HydrEpoxy 300. The squares were exposed to 2.5 W/cm^2 radiant heat with pilot flame.

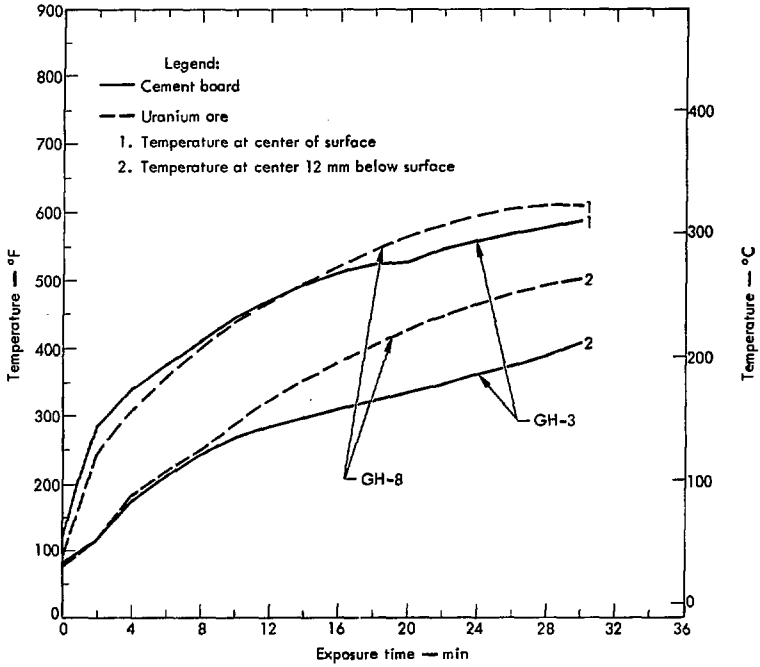

Fig. A-4. Surface and body temperatures of cement-board and uranium-ore squares whose front surface had been coated with 10 mils of HydrEpoxy 300. The squares were exposed to 2.5 W/cm^2 radiant heat, without pilot flame.

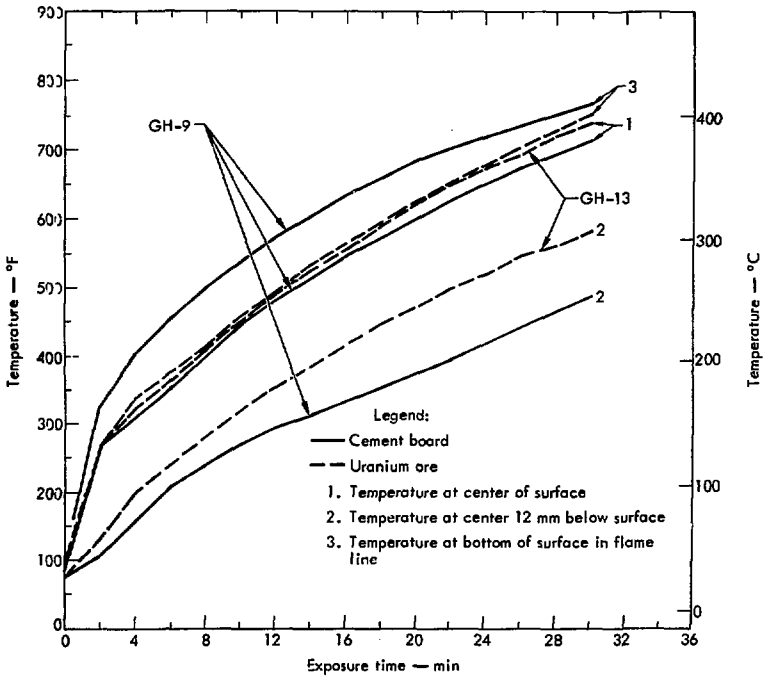

Fig. A-5. Surface and body temperature of cement-board and uranium-ore squares whose front surface was coated with 10 mils of Saran XD-7151. The squares were exposed to 2.5 W/cm^2 radiant heat with pilot flame.

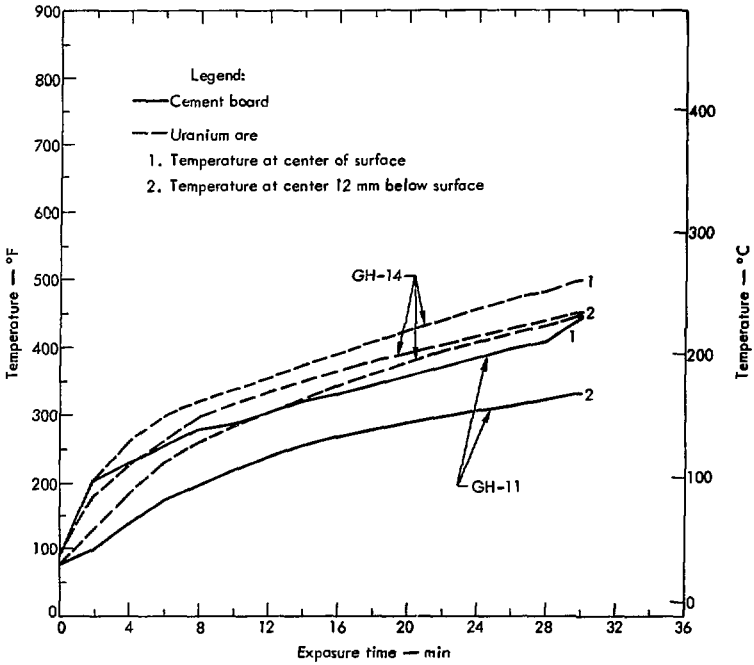

Fig. A-6. Surface and body temperature of cement-board and uranium-ore squares whose front surface was coated with Saran XD-7151. The squares were exposed to 2.5 W/cm^2 radiant heat, without pilot flame.

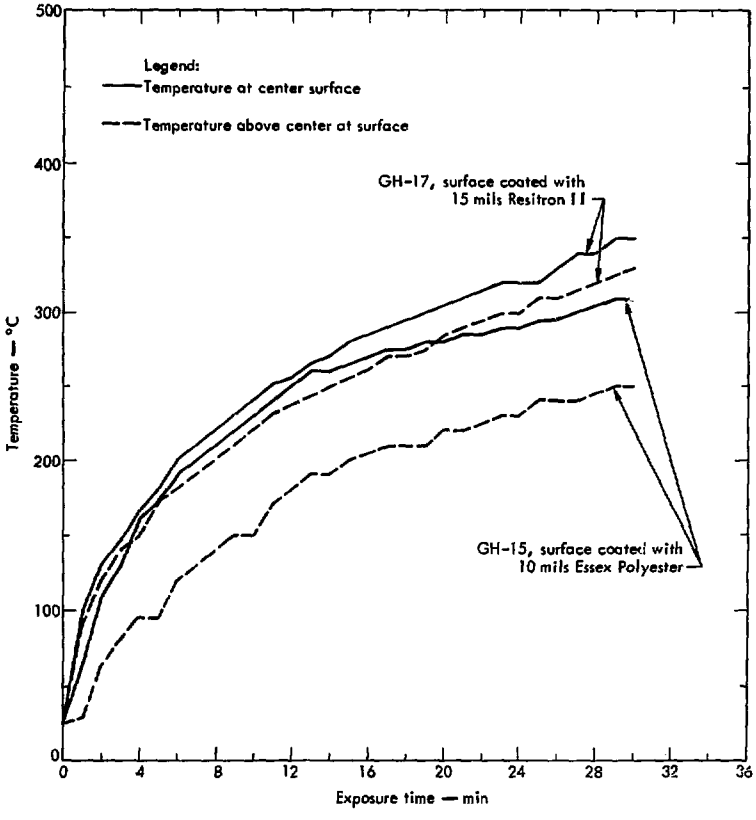

Fig. A-7. Surface and body temperature of sample exposed to 2.5 W/cm^2 radiant heat without pilot flame.

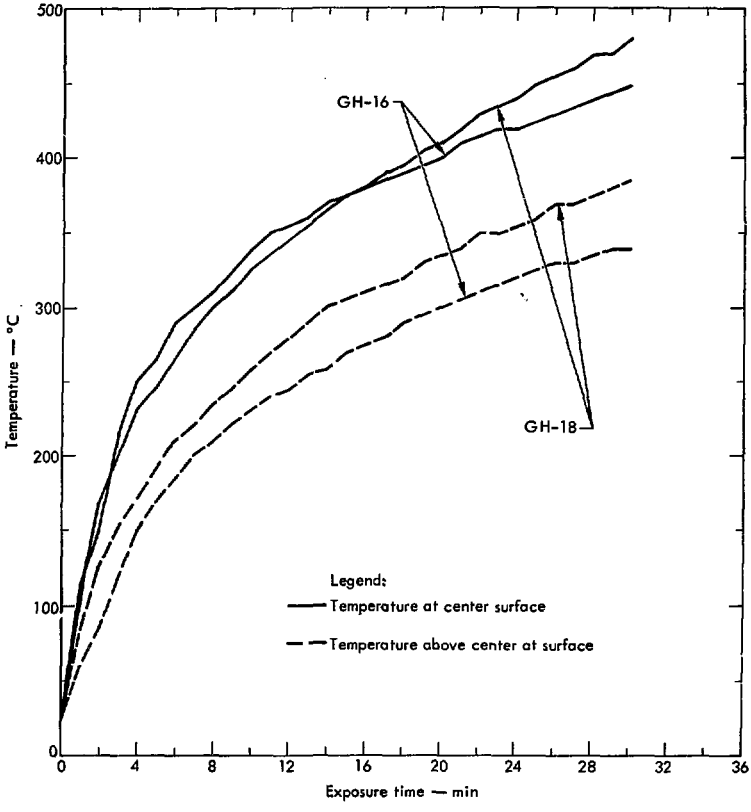

Fig. A-8. Surface and body temperature of sample exposed to 2.5 W/cm^2 radiant heat with pilot flame.

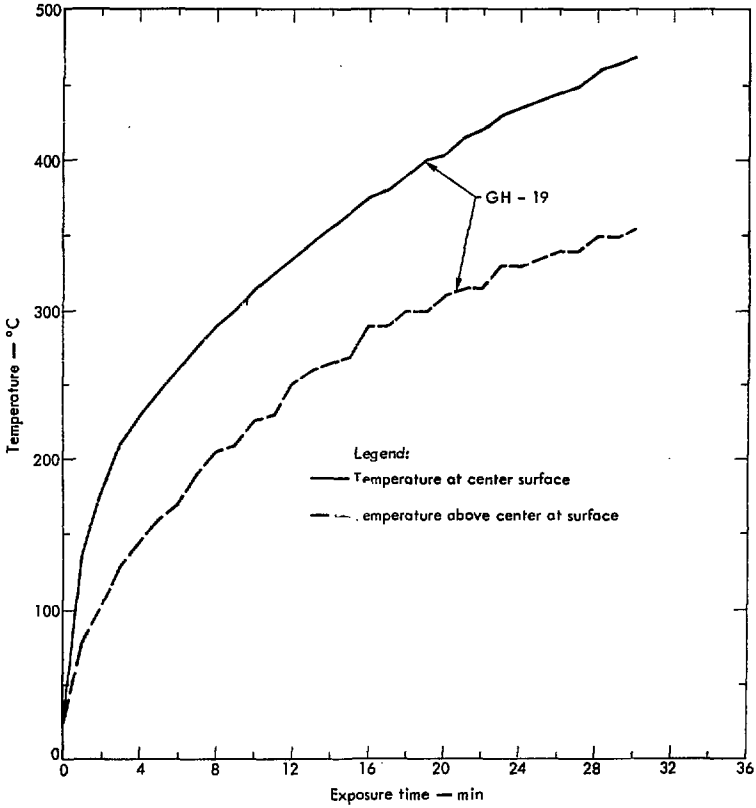

Fig. A-9. Surface and body temperature of sample GH-19, surface coated with 20 mils Resitron II and exposed to 2.5 W/cm^2 radiant heat with pilot flame.

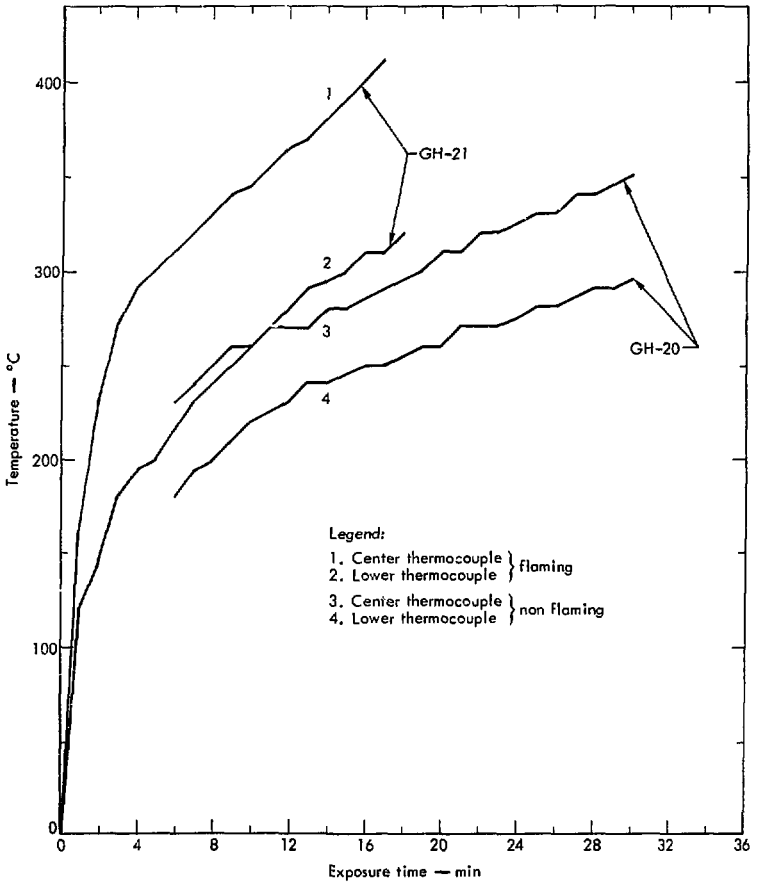

Fig. A-10. Surface and body temperature of a sample whose surface was coated with WSU-118 and exposed to 2.5 W/cm^2 radiant heat with and without flame.

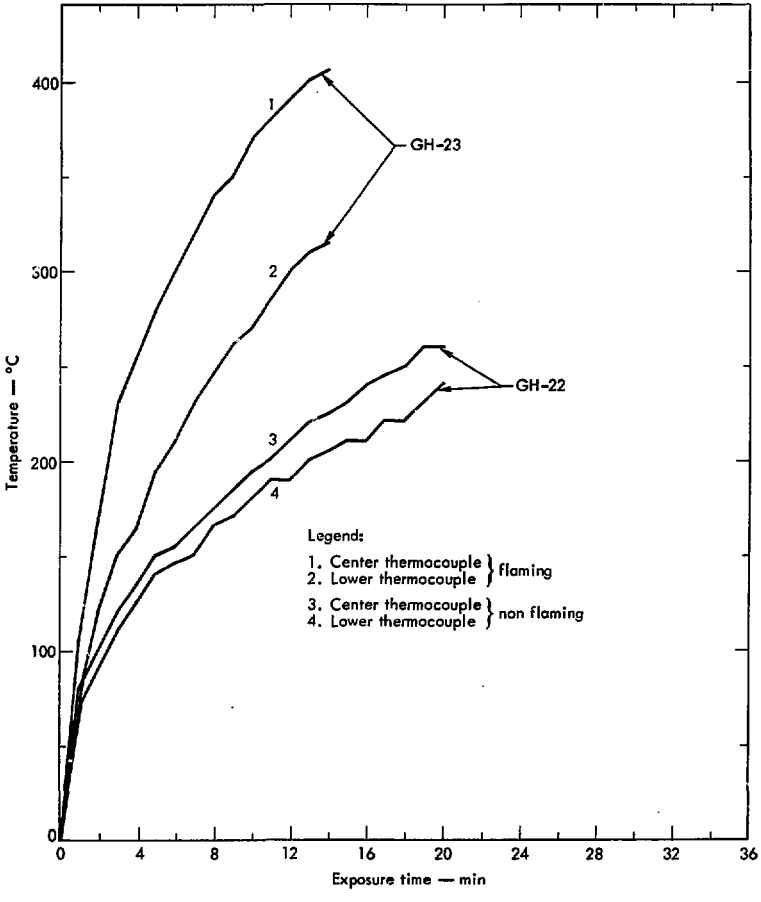

Fig. A-11. Temperatures recorded at the center and lower thermocouple of a sample coated with Aerospray 70 and exposed to 2.5 W/cm^2 of radiant heat with and without flame.

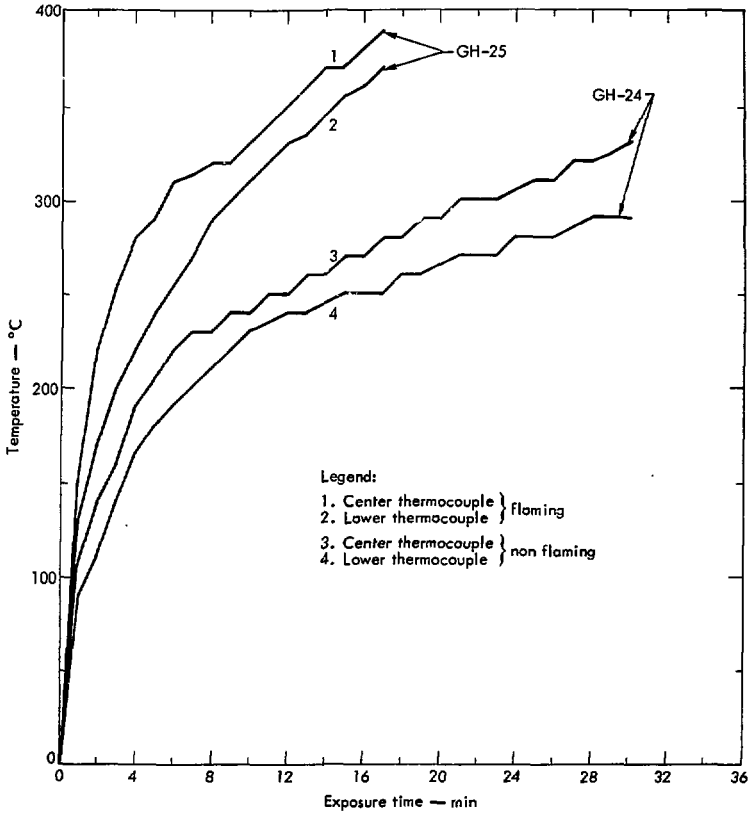

Fig. A-12. Temperatures recorded at the center and lower thermocouple of a sample coated with EpiRez WD-510/ EpiCure 872 and exposed to 2.5 W/cm^2 of radiant heat with and without flame.

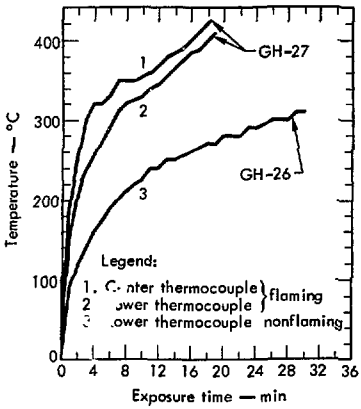

Fig. A-13. Temperatures recorded at the center and *lower thermocouple of a sample coated* with EpiRez WD-510/EpiCure 872 and 879. The sample was exposed to 2.5 W/cm^2 of radiant heat with and without flame.

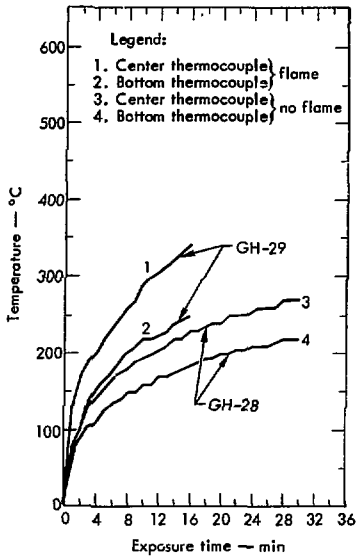

Fig. A-14. Temperatures at the center and bottom of samples coated with Promulsion 200.

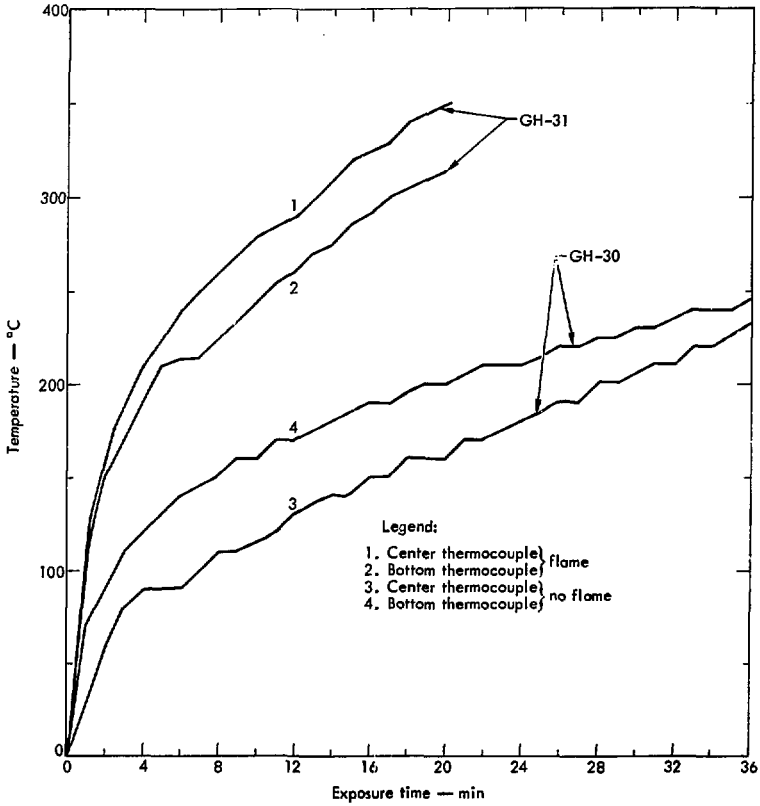

Fig. A-15. Temperatures at the center and bottom of samples coated with Hydro Seal.

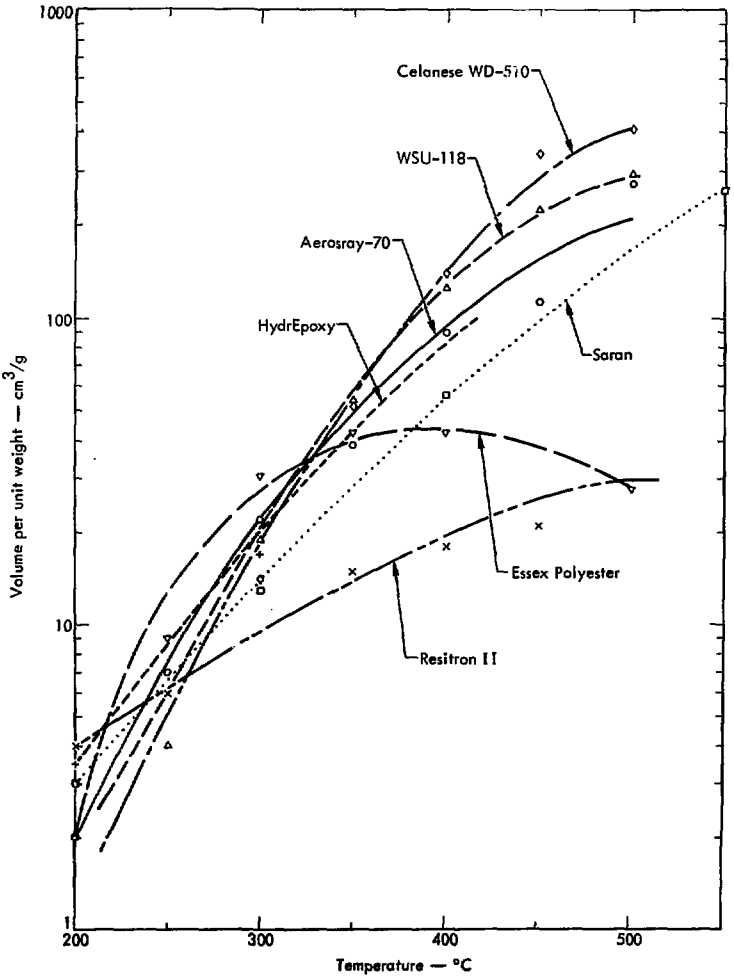

Fig. A-16. Carbon monoxide evolution.

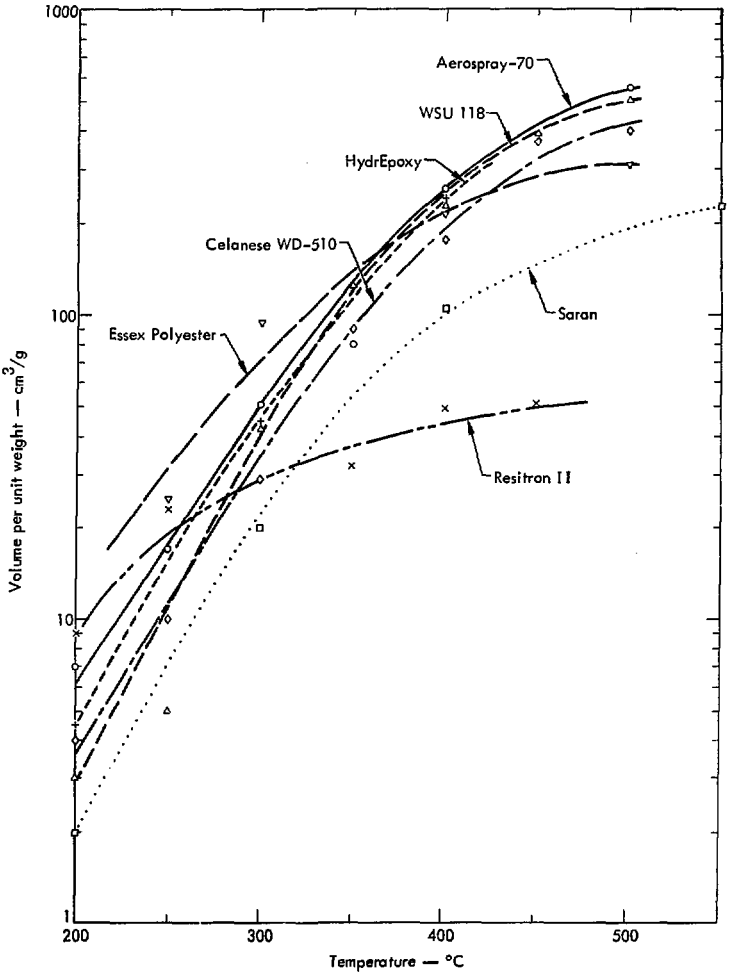

Fig. A-17. Carbon dioxide evolution.

Appendix B:

Computer Program (PDP-8) for Calculation of Permeability Coefficients from Dow Cell Data

```
.R PERM
?00.00
*W A
C POLYMERIC MATERIALS LOCAL  -  7/18/73

01.01 T "PERMEABILITY PROGRAM.",!
01.02 C FILE PERM.SV  1/9/74
01.03 T "ENTER UNITS PER ASTM-D-1434-66 METHOD M.",!!
01.05 C PROGRAM TO COMPUTE GAS TRANSMISSION THROUGH THIN FILMS.
01.07 CHANGE DATE 8-17-73
01.10 S A=1.872
01.20 S AT=63.62
01.30 A "H (MM) = ",H
01.40 S HR=65.5
01.50 S HL=65.5
01.60 A "P (MMHG) = ",P
01.70 S T=296
01.80 A "VF (MM↑3) = ",VF
01.90 A "RTC (MMHG/IN↑-1) = ",RC
01.95 A "RTP (IN/H) = ",RP
01.96 S T1=0

02.10 A "SLP (IN(MMHG)/IN(H)) = ",SP
02.20 A "T1 (THICKNESS OF CARRIER - MIL) = ",T1
02.30 A "T3 (THICKNESS OF SAMPLE - MIL) = ",T3
02.40 I (T1) 2.5,3.1,2.5
02.50 A "PC (PERM. OF CARRIER) = ",PC

03.10 S PT=HL-H;S DH=(RC*RP)/SP
03.20 S GR=(4.09*10↑12/((P-PT)*AT))*DH
03.30 S GR=GR*(((2*A*H)-(A*(HL+HR))-VF)/(6.23*10↑7)*T)
03.40 S PM=GR*T3*(3.87/10↑14)
03.50 I (T1) 3.6,4.1,3.6
03.60 S T2=(T3-T1)/10↑3;S T4=T1/10↑3;S T5=T3/10↑3
03.70 S PL=(T2*PM*PC)/((T5*PC)-(T4*PM))

04.10 T !,"GTR = ",%6.06,GR,!
04.20 T "PERM OF SAMPLE = ",%,PM,%6.06,!
04.30 IF (T1) 4.4,4.9,4.4
04.40 T "PERM OF COATING = ",%,PL,%6.06,!
04.90 T !!;S CT=10;G 10.1
```

```
10.10 A "CHANGE - ",CH
10.20 I (CT) 10.3,10.4
10.30 I (CH) 10.4,19.1
10.40 I (CH) 10.5,3.1
10.50 S CT=0
10.80 I (CH-0H) 11.2,14.3

11.20 I (CH-0P) 11.4,14.6
11.40 I (CH-0VF) 11.5,14.8
11.50 I (CH-0RTC) 11.6,14.9
11.60 I (CH-0RTP) 11.7,15.1
11.70 I (CH-0SLP) 11.8,15.2
11.80 I (CH-0T1) 11.9,15.3
11.90 I (CH-0T3) 12.1,15.4

12.10 I (CH-0PC) 12.2 15.5
12.20 T "? ? ?",1;G 10.1

14.30 D 1.3;G 10.1
14.60 D 1.6;G 10.1
14.80 D 1.8;G 10.1
14.90 D 1.9;G 10.1

15.10 D 1.95;G 10.1
15.20 D 2.1;G 10.1
15.30 D 2.2;D 2.5;G 10.1
15.40 D 2.3;G 10.1
15.50 D 2.5;G 10.1

19.10 Q
*701.00
*701.00
*
```

Appendix C:*

Direct Determination of Radon Permeability Through Polycarbonate Film

In connection with the program to find sealants for uranium mine tunnels, an experiment to determine the permeation of radon-222 through polycarbonate (PC) film was performed. The cell used in the experiment is shown in Fig. C-1.

The two halves of the cell were constructed of 80-mm Pyrex glass tubing. This tubing has an inner diameter of 74 mm and the exposed area of the membrane mounted between the two halves was thus 43 cm^2. The volume of the upper half of the cell was about 200 cm^3 and the lower half about 20 cm^3. The flanges of the cell were greased with Apiezon N and a square portion of the membrane about 10 cm on a side mounted between them. The two halves of the cell were wired together and then simultaneously evacuated to check that a vacuum-tight seal had been obtained. Once this was confirmed, air was simultaneously admitted to the two halves of the cell to a pressure of about 70 cm Hg (93 kPa).

A flask of about 400 cm^3 volume containing about 100 cm^3 of a solution of about 10^9 DPM of radon-226 had been previously evacuated and allowed to stand for a month until the 3.8-day radon-222 had grown into equilibrium. The flask was attached to the vacuum manifold and filled with air to a pressure of about 70 cm Hg (93 kPa). Subsequent to the experiment, samples of the gas were taken and the atoms of radon-222 per unit volume determined by alpha-counting.

The experiment was initiated by attaching the radon-226 flask to the lower cell and opening stopcocks to admit the radon-222 to the lower side of the membrane. Initially both halves of the cell contained a total pressure of about 70 cm Hg, and once radon-222 air diffusion from the flask to the lower cell was complete, the "pressure" of radon-222 on the lower side of the cell would be constant.

Referring to Fig. C-1, helium from the upper left port was periodically flushed through the upper cell and into the U-trap packed with molecular sieve 5A. The MS5A trap was cooled in liquid nitrogen during these sampling operations. Pumping on the trap exit at upper right maintained pressure at 96 ± 1.3 kPa. While there is no stable isotopic carrier for radon-222, ethane has similar adsorption characteristics on MS5A. Approximately 30 cm^3_{STP} (0°C, 101 kPa) of ethane were added to each collected radon-222 fraction and the mixture desorbed at 350°C into a liquid nitrogen cooled trap. Counting tubes were calibrated on the alpha plateau using the radon-222 at equilibrium with a known amount of radon-226. By expanding a known amount of the radon-222 ethane mixture into one of these tubes and counting radon-222, one determines the radon-222 per unit volume of mixture. From the known total of the mixture one then calculates total radon-222 in the sample. Measurements were made at least in duplicate. The percent errors quoted in the table of results are standard deviations based on the differences among replicates.

The experiment extended over a period of 32 days during which 14 collections of radon-222 from the upper cell were made. The results are given in Table C-1. Columns 1 and 2 list sample number and sampling time. Column 3 gives the number of atoms in the sample at sampling time per cm^2 of exposed membrane. As noted above, this area was 43 cm^2. Column 4 gives a cumulative total obtained by summing the atoms per cm^2 in the latest sample and those in all previous samples decay-corrected to the latest time of sampling. These results are thus the total which would have been observed in the sample if no prior sample had been taken. It will be seen later that this is one of the easier quantities to calculate theorectically. The half-life of radon-222 was taken as 3.82 days. Columns 5, 6, and 7 will be elucidated later.

---

*The work reported in this section was done and reported by Floyd Momyer.

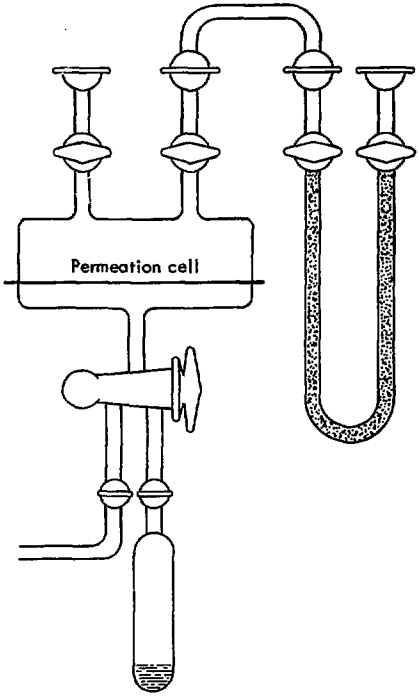

Fig. C-1. Schematic of radon-222 permeation cell and experimental setup.

Table C-1. Results for Radon-222 Permeation Through Polycarbonate.[a,b]

Sample	Time, h	Atoms/sample[c]	Σ Atoms[c]	C_1 (Q)	C_1 (S)	C_1 (R)
1	2.42	6.25×10^{2} 4.9%	6.25×10^{2}	—	—	—
2	69.43	4.99×10^{6} 1.5%	4.99×10^{6}	3.23×10^{11}	3.23×10^{11}	(4.32×10^{10})
3	74.18	1.73×10^{6} 1.1%	6.54×10^{6}	3.19×10^{11}	3.07×10^{11}	(1.60×10^{11})
4	96.82	1.07×10^{7} 2.9%	1.62×10^{7}	2.93×10^{11}	2.82×10^{11}	(1.73×10^{11})
5	141.53	3.14×10^{7} 0.4%	4.30×10^{7}	2.76×10^{11}	2.70×10^{11}	(2.09×10^{11})
6	165.87	2.29×10^{7} 0.4%	5.86×10^{7}	2.71×10^{11}	2.64×10^{11}	(2.39×10^{11})
7	237.80	7.86×10^{7} 2.0%	1.13×10^{8}	3.01×10^{11}	3.16×10^{11}	2.98×10^{11}
8	288.53	7.21×10^{7} 0.8%	1.49×10^{8}	3.26×10^{11}	(3.58×10^{11})	(3.52×10^{11})
9	333.98	5.56×10^{7} 0.4%	1.61×10^{8}	3.15×10^{11}	2.97×10^{11}	2.95×10^{11}
10	405.85	8.53×10^{7} 1.2%	1.79×10^{8}	3.14×10^{11}	3.13×10^{11}	3.12×10^{11}
11	477.23	9.10×10^{7} 1.8%	1.95×10^{8}	3.23×10^{11}	3.34×10^{11}	3.34×10^{11}
12	573.77	1.06×10^{8} 0.8%	2.00×10^{8}	3.18×10^{11}	3.13×10^{11}	3.13×10^{11}
13	764.77	1.50×10^{8} 1.7%	1.98×10^{8}	3.05×10^{11}	3.01×10^{11}	3.01×10^{11}
14	766.27	2.64×10^{6} 2.6%	1.98×10^{8}	3.05×10^{11}	(3.58×10^{11})	(3.58×10^{11})
				3.07×10^{11} 5.8%	3.02×10^{11} 7.3%	3.09×10^{11} 4.7%

[a] $D = 5.28 \times 10^{-11}$ cm^2/s in calculations.

[b] The resulting best value for C_1 is 3.06×10^{11} atoms radon-222 per cm^3 of polycarbonate at the coating – radon-222 interface.

[c] At sample time per cm^2.

If the concentration in the membrane is given by a function C (x,t), then for a stable species the boundary value problem we are interested in is:

$$\frac{\partial C}{\partial t} = D\frac{\partial^2 C}{\partial x^2} \tag{1}$$

$$C(x,0) = 0, 0 < x < \ell \tag{2}$$

$$C(0,t) = C_1 \text{ , all t} \tag{3}$$

$$C(\ell,t) = 0, \text{ all t} \tag{4}$$

In the above, x = distance into the film, ℓ = total thickness of the film, t = time. D = the diffusion constant of the species in the membrane, C(x,t) = atoms per unit volume of membrane at given x and t, and C_1 is the (constant) concentration in the membrane at the x = 0 interface.

If one assumes that C_1 is proportional to pressure (Henry's law), then $C_1 = KP$, where C_1 is the concentration in $\frac{cm^3_{STP}\ ^{222}Rn}{cm^3 \text{ membrane}}$, P is the pressure of radon-222 on the upstream side in kPa, and K is the solubility (Henry's law constant) in units of $\frac{cm^3_{STP} \text{ of } ^{222}Rn/cm^3 \text{ membrane}}{kPa \text{ of } ^{222}Rn}$.

If we call this solution $C^0(x,t)$, then:

$$C^0(x,t) = C_1\left(1 - \frac{x}{\ell}\right) - \frac{2C_1}{\pi}\sum_{n=1}^{\infty}\frac{1}{n}\sin\frac{n\pi x}{\ell}\, e^{-\frac{Dn^2\pi^2 t}{\ell^2}} \tag{5}$$

However, for a radioactive species the decay law says dN/dt = $-\lambda N$, where N is the number of atoms present at a given time, and λ is the disintegration constant of the diffusing species. Thus, if C(x,t) is the number of atoms per unit volume present in the membrane, the differential Eq (1) must be modified to

$$\frac{\partial C}{\partial t} = D\frac{\partial^2 C}{\partial x^2} - \lambda C \ . \tag{1a}$$

The other conditions remain the same. Following Carslaw and Jaeger*

$$C(x,t) = \lambda\int_0^t e^{-\lambda t'}C^0(t')dt' + C^0 e^{-\lambda t} ,$$

where $C^0(x,t)$ is the function given above, and t' is a variable of integration.

The result of this integration is

$$C = C_1\left(1 - \frac{x}{\ell}\right) - \frac{2C_1\lambda\ell^2}{D\pi^3}\sum_{n=1}^{\infty}\frac{1}{n}\sin\frac{n\pi x}{\ell}\left\{\frac{1 + \frac{D\pi^2 n^2}{\lambda\ell^2}\, e^{-\left(\frac{D\pi^2 n^2}{\ell^2} + \lambda\right)t}}{n^2 + \frac{\lambda\ell^2}{D\pi^2}}\right\} . \tag{6}$$

---

*H.S. Carslaw and J.C. Jaeger, Conduction of Heat in Solids (Oxford Press, 1959) p. 33; also Danckwertz, Trans. Faraday Soc. 47 (1951) 1014-23.

Also if q is the rate of passage of atoms across the plane at x, then

$$q = -D\frac{\partial C}{\partial x}$$

and

$$q = \frac{DC_1}{\ell} + \frac{2C_1\lambda\ell}{\pi^2}\sum_{n=1}^{\infty}\cos\frac{n\pi x}{\ell}\left\{\frac{1 + \frac{D\pi^2 n^2}{\lambda\ell^2}\, e^{-\left(\frac{D\pi^2 n^2}{\ell^2}+\lambda\right)t}}{n^2 + \frac{\lambda\ell^2}{D\pi^2}}\right\} . \tag{7}$$

The above equation is, of course, generally evaluated at $x = \ell$ where $\cos\frac{n\pi x}{\ell} = (-1)^n$. It should be noted at this point that for $\lambda = 0$ the late time rate of permeation at $x = \ell$ is simply

$$(q)_{x=\ell} = \frac{DC_1}{\ell} .$$

However, for a finite disintegration constant, at late times

$$(q)_{x=\ell} = \frac{DC_1}{\ell}\cdot\frac{\sqrt{\frac{\lambda}{D}}\cdot\ell}{\sinh\left\{\sqrt{\frac{\lambda}{D}}\cdot\ell\right.} . \tag{8}$$

Evaluation of the series in the second member on the right shows this member to be always negative. In fact, depending upon values of D, λ, and ℓ the first and second members may be comparable in absolute value. One may think of this as meaning that, on the average, the time an atom spends in the membrane after leaving the constant source of supply and before emerging on the other side may be significant compared to its radioactive lifetime. Unfortunately, this "holdup" time does not appear to be a very simple function of the parameters involved. However, the result is that the effect of a membrane in reducing downstream concentration of a radioactive species is always enhanced by radioactive decay – and this effect may be quite significant. The late-time rate of permeation is still a simple linear function of C_1; however, it is no longer inversely proportional to thickness but decreases more strongly with increase in thickness. The product of solubility and diffusion constant no longer determines late-time rate of permeation. *Unless films having extremely low solubility are found, the diffusion constant alone is the critical parameter.*

To proceed with the solution of the boundary value problem, observations were actually made on the amount of radon-222 existing on the downstream side at various times. If the amount having crossed the plane x and existing at a time T is Q, then

$$Q = \int_0^T q(t)e^{-\lambda(T-t)}\,dt = e^{-\lambda T}\int_0^T q(t)e^{\lambda t}\,dt .$$

The result of this integration is

$$Q = \frac{DC_1}{\lambda\ell}(1 - e^{-\lambda T}) + \frac{2C_1\ell}{\pi^2}\sum_{n=1}^{\infty}\cos\frac{n\pi x}{\ell}\left\{\frac{1 - e^{-\left(\frac{D\pi^2 n^2}{\ell^2}+\lambda\right)T}}{n^2 + \frac{\lambda\ell^2}{D\pi^2}}\right\} . \tag{9}$$

Again, at late time and for $x = \ell$ the total radon-222 existing on the far side of the film is

$$(Q)_{x=\ell} = \frac{DC_1}{\lambda\ell} \cdot \frac{\sqrt{\frac{\lambda}{D}} \cdot \ell}{\sinh\left\{\sqrt{\frac{\lambda}{D}} \cdot \ell\right.} \quad . \tag{10}$$

Thus, not only the rate of permeation eventually becomes constant, but the total radon-222 existing on the downstream side of the membrane is constant. It will also be noted that $(q)_{x=\ell} = \lambda(Q)_{x=\ell}$ at late times, as it should when the rate of entrance into the downstream region finally equals the rate of decay of those atoms already downstream.

Before attempting interpretation of the results, several comments on departures from the theory on which the interpretation will be based should be made. While in principle these departures are all correctable, it was decided to design the experiment on the basis of convenience and maximum utilization of existing equipment with the aim of obtaining results uncertain by less than the factor of two that we understood was acceptable.

The first violation of the boundary conditions used in the solution of the differential equation for the permeation process is that the concentration of radon-222 on the upper side of the membrane is not always zero. Intuitively, one would expect that after a long interval between samplings the observed rate of permeation would be depressed and that a period of increased permeation would follow sampling. It will be seen that the next-to-last sampling interval was nearly 200 h and the last 1.5 h. While the last sample does indeed show an increased rate of permeation beyond analytical error, the effect is in any case less than 20%.

The temperature was not rigorously controlled in the box containing the equipment. However, periodic logging of the box temperature indicated that it remained within the range (21 ± 2)°C.

At the initiation of the experiment, the pressure at the lower side of the membrane was not constant until interdiffusion of air and radon-222 was complete in the lower cell. Since this process should take hours and the experiment ran hundreds of hours this was considered acceptable.

Similarly, the reduction of radon-222 pressure in the radon-226 flask by an initial sampling operation was considered acceptable on the time scale of the experiment since equilibrium would be reestablished to within a fraction of a percent within a week.

One worries about the possibility of pinholes in the membrane, also the 10^9 DPM solution of radon-226 was at least connected to the vacuum system to fill it with air prior to the experiment. Although care was taken in this operation, the possibility of contamination in the vacuum system could not be ruled out. The first sample at 2.42 h was taken as a check on these possibilities. Theory says there should be no detectable radon-222 in this sample. Whether the value reported is real is not unambiguous since the observations in the counting tubes were a few tenths of a count per minute over about one count per minute background. In any case, the observed amount is 4 orders of magnitude less than that in any subsequent sample. Thus leaks or contamination appear to have been at acceptable levels.

There are a number of ways in which one can handle the results of this experiment.

Method 1

In the first place, as was done in Table C-1, one can sum all samples suitably decay-corrected to obtain the total permeation at the time of a given sample. This has two advantages. Inspection of the equation for $(Q)_{x=\ell}$

indicates that at late times Q becomes an approximately linear function of the parameter $\tau = 1 - e^{-\lambda T}$. If τ^0 is the intercept of this line with the τ axis, then

$$D = \frac{2\ell^2\lambda}{\pi^2\tau^0} \sum_{n=1}^{\infty} \frac{(-1)^n}{n^2 + \frac{\lambda\ell^2}{D\pi^2}} \quad . \tag{11}$$

Such a plot was indeed made on data from the last eight samples to obtain a least-squares fit for the late Q = 0 intercept, and a value of D was calculated from this intercept.

Once the value of D is known it will be seen that the data from the experiment can be used to derive a value of C_1 from total permeation at each sampling. Since C_1 is assumed to be a constant, the above value obtained graphically for D was taken as the starting point for an iterative routine on D that resulted in the least sum of squares about the mean for C_1 for all but the initial sample. This process resulted in a value for D about 10% lower than the original estimate. Figure C-2 presents the data as a function of τ. The theoretical curves (solid lines) are from the result for D of the iterative process.

The second advantage of this mode of presentation is that the results should be a smooth curve plotted against time which can be compared with a theoretical curve. Figure C-3 is a plot of the experimental data compared to a theoretical curve derived from final values of the parameters D and C_1.

It might be noted that for $D = 5.28 \times 10^{-11}$ cm^2/s, the average for C_1 in 12 samples is 3.06×10^{11} 5.8%. If D is increased 10%, C_1 from these same samples is 2.39×10^{11} 11.3%, and individual values show a distinct upward trend with increasing sampling time. Decreasing D by 10% results in C_1 equal to 4.15×10^{11} 14.3% and a downward trend with increasing time.

The disadvantage of this procedure is that an error in any one of the previous samples will be propagated until radioactive decay has reduced it to insignificance.

Method 2

The data can also be used to calculate a value of C_1 from the number of atoms in each sample. Thus, if s refers to the number of the sample,

$$Q_s = Q_{T_s} - Q_{T_{s-1}} e^{-\lambda(T_s - T_{s-1})} .$$

Regarding the data in this manner suggests that sample 8 is too high by about 15%, probably due to an error in the amount of ethane carrier added to the radon-222. Results from the other data would allow correction for this, and such calculations were performed. Since they made less than 1% difference in the final conclusions, the data are presented as obtained. Such an error is considered insignificant compared to other uncertainties in the experiment.

Method 3

A third method of treating the data is suggested by noting that once the rate of permeation (q) is constant, the radon-222 in each sample satisfies the equation

$$q = \frac{\lambda Q_s}{1 - e^{-\lambda(T_s - T_{s-1})}} \quad . \tag{12}$$

Thus, once the value of D has been determined, a value of C_1 can again be calculated from the result of each sampling.

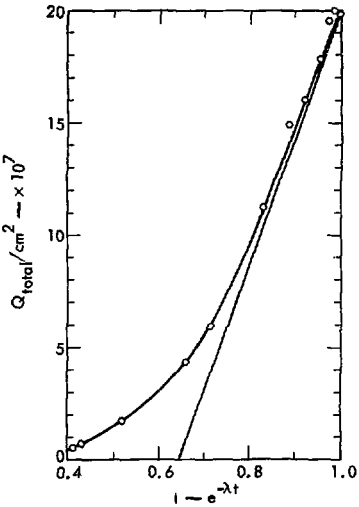

Fig. C-2. Total permeation vs $1 - e^{-\lambda t}$

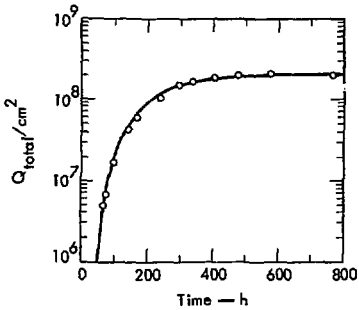

Fig. C-3. Total permeation vs time.

It might be noted that once steady-state has been achieved, methods two and three are equivalent in principle.

For purposes of data reduction, a program was written for the CDC 7600 which would calculate q/C_1 and Q/C_1 at $x = \ell$ as a function of λ, D, ℓ, and t. The disintegration constant, λ, was taken throughout as 7.55×10^{-3}/h. At early times all of these series, particularly that for q, are not very well behaved. Thus, calculations on q at early times are suspect both for calculational reasons and the fact that q is actually increasing during the early sampling intervals. All values of rate of permeation calculated will be too small, and yield a low value for C_1. Although fewer terms would suffice in most instances, calculations were rather arbitrarily based on the first 5000 terms of each of the series since this required only about a second of computer time.

Referring back to Table C-1, column 5 lists derived values of C_1 (Q) based on method 1 above, or total permeation to sample time. Column 6 lists values of C_1(s) based on method 2 or the permeation in each sample. Column 7 lists values of C_1 derived from method 3, or rate of permeation during each interval. It will be noted that the values in column 7 are indeed less than those in column 6 at early times, and later approach them almost exactly. Parenthesized values were not used in calculating quoted averages.

The samples taken at the end of the experiment indicated 1.09×10^{10} 1.5% atoms of radon-222 per cm^3 of flask volume or a pressure of radon-222 = 4.44×10^{-5} Pa at 21°C. For $D = 5.28 \times 10^{-11}$ cm^2/s, the value, C_1, of the concentration in the membrane at x = 0 is 3.06×10^{11} atoms $^{222}Rn/cm^3$ PC or 1.138×10^{-8} cm^3_{STP} ^{222}Rn per cm^3 of PC. Assuming Henry's law,

$$C_1 = \left(0.257 \frac{cm^3_{STP}\ ^{222}Rn/cm^3\ PC}{kPa\ ^{222}Rn}\right) \times P\ (kPa)\ of\ ^{222}Rn.$$

Alternatively,

$$\frac{atoms\ ^{222}Rn}{cm^3\ PC} = 28.0 \times \frac{atoms\ ^{222}Rn}{cm^3\ void}$$

To illustrate the effect of radioactive decay, one may use Eq (8) to calculate late time permeation as a function of ℓ. He may also calculate permeation for a stable species with the same values of D and C_1. Figure C-4 is a plot of the results. The ordinate is atoms/cm^2/h (into the tunnel) per atoms/per cm^3 void (in the mine wall). For radon-222 this ratio has the same numerical value if one expresses radon-222 in disintegrations per minute (DPM). The thickness of the film in this experiment (0.137 mm) is marked on the plot.

Given a thickness of 0.137 mm for the membrane, Fig. C-5 is a plot of total atoms of radon-222 downstream per atom/cm^3 upstream, and rate of permeation (per hour) of radon-222 per atom per cm^3 upstream.

A previous experiment extending over 5 h failed because the diffusion constant was almost two orders of magnitude less than expected. In an attempt to gain information for planning the current experiment, the alpha-activity remaining in the foil was determined with a survey meter at various times for two weeks after removal from the radon-222 source. From the observed "half-life", a value of 4.6×10^{-11} cm^2/s was calculated for D. These were crude measurements and this is quite good agreement with the current best value 5.28×10^{-11} cm^2/s. Even with more sophisticated counting techniques, the determination of total radon-222 in the film (and thus solubility) is complicated by the fact that the film corresponded to 2 to 3 ranges for the alpha-particles involved. This makes absolute counting efficiency very difficult to determine.

However, these observations suggest an attractive technique for determining diffusion constant and solubility of radon-222 in membranes. For films "thin" compared to alpha-particle ranges, the counting efficiency is known. One is speaking generally of films about 1 mil in thickness. One could expose a membrane (or a number of membranes) to a constant known pressure of radon-222 until saturation is reached. The membrane(s) could then be removed from the source and total radon-222 determined as a function of time by alpha-counting. For the class

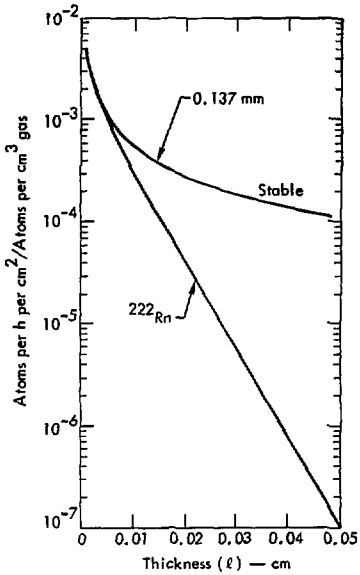

Fig. C-4. Steady-state permeation vs thickness (ℓ).

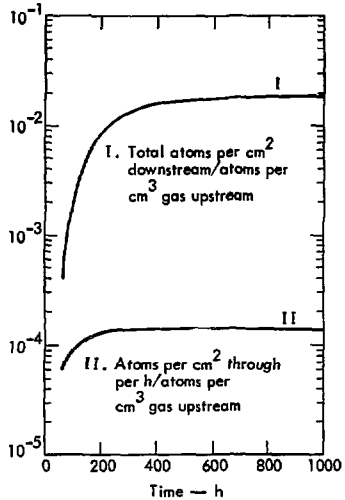

Fig. C-5. Total permeation and rate of permeation vs time.

of substances with low diffusion constants, theory would then allow determination of both diffusion constant and solubility.

We have the following boundary value problem :

$$\frac{\partial C}{\partial t} = \frac{D\partial^2 C}{\partial x^2} - \lambda C$$

$$C(x,0) = C_1 . 0 < x < \ell$$

$$C(0,t) = 0, \text{ all } t$$

$$C(\ell,t) = 0, \text{ all } t \ .$$

A substitution, $C = \mu e^{-\lambda t}$, results in

$$\frac{\partial \mu}{\partial t} = \frac{D\partial^2 \mu}{\partial x^2} \ . \tag{1a}$$

Other boundary conditions on μ remain the same.
Ultimately, the solution for C is

$$C = \frac{4 C_1 e^{-\lambda t}}{\pi} \sum_{n=1}^{\infty} \frac{\sin\left\{\frac{(2n-1)\pi x}{\ell}\right\}}{(2n-1)} e^{-\frac{D(2n-1)^2\pi^2 t}{\ell^2}} \ . \tag{13}$$

Also, Q, the amount in the membrane at a given time is

$$Q = \int_0^{\ell} C dx = \frac{8 \ell C_1 e^{-\lambda t}}{\pi^2} \sum_{n=1}^{\infty} \frac{e^{-\frac{D(2n-1)^2\pi^2 t}{\ell^2}}}{(2n-1)^2} \ . \tag{14}$$

This series converges quite rapidly so that one approaches

$$Q = \frac{8\ell C_1}{\pi^2} e^{-\left(\frac{D\pi^2}{\ell^2} + \lambda\right) t} \ . \tag{15}$$

Q (t) can be determined directly by alpha-counting the membrane at a series of times. From its dependence on time, the argument of t in the exponential can be determined. As ℓ and λ are known, D can thus be calculated. Also, once the argument of t is known a value of C_1 can be calculated from each alpha-count. For values of D and ℓ leading to a time argument corresponding to a "half-life" of less than a few hours, the presence of the daughters polonium-218 and polonium-214 of radon-222, introduces some complication in the calculations as their alpha-particles will also be counted. However, this can be handled in a straightforward manner.